

RESEARCH ARTICLE

10.1002/2015JD024066

Key Points:

- Strong bromide depletion relative to sodium in Antarctic sea-salt aerosol
- No significant bromine snow emission over Antarctica
- Significant sea-salt contributions from sea ice and open ocean sources

Correspondence to:

M. Legrand,
legrand@lgge.obs.ujf-grenoble.fr

Citation:

Legrand, M., X. Yang, S. Preunkert, and N. Theys (2016), Year-round records of sea salt, gaseous, and particulate inorganic bromine in the atmospheric boundary layer at coastal (Dumont d'Urville) and central (Concordia) East Antarctic sites, *J. Geophys. Res. Atmos.*, *121*, 997–1023, doi:10.1002/2015JD024066.

Received 8 AUG 2015

Accepted 22 DEC 2015

Accepted article online 29 DEC 2015

Published online 23 JAN 2016

Year-round records of sea salt, gaseous, and particulate inorganic bromine in the atmospheric boundary layer at coastal (Dumont d'Urville) and central (Concordia) East Antarctic sites

Michel Legrand^{1,2}, Xin Yang³, Susanne Preunkert^{1,2}, and Nicolas Theys⁴

¹Laboratoire de Glaciologie et Géophysique de l'Environnement, University Grenoble Alpes, Grenoble, France, ²LGGE UMR 5183, CNRS, Grenoble, France, ³British Antarctic Survey, Natural Environment Research Council, Cambridge, UK, ⁴Belgium Institute for space Aeronomy (IASB-BIRA), Brussels, Belgium

Abstract Multiple year-round records of bulk and size-segregated compositions of aerosol were obtained at the coastal Dumont d'Urville (DDU) and inland Concordia sites located in East Antarctica. They document the sea-salt aerosol load and composition including, for the first time in Antarctica, the bromide depletion of sea-salt aerosol relative to sodium with respect to seawater. In parallel, measurements of bromide trapped in mist chambers and denuder tubes were done to investigate the concentrations of gaseous inorganic bromine species. These data are compared to simulations done with an off-line chemistry transport model, coupled with a full tropospheric bromine chemistry scheme and a process-based sea-salt production module that includes both sea-ice-sourced and open-ocean-sourced aerosol emissions. Observed and simulated sea-salt concentrations sometime differ by up to a factor of 2 to 3, particularly at DDU possibly due to local wind pattern. In spite of these discrepancies, both at coastal and inland Antarctica, the dominance of sea-ice-related processes with respect to open ocean emissions for the sea-salt aerosol load in winter is confirmed. For summer, observations and simulations point out sea salt as the main source of gaseous inorganic bromine species. Investigations of bromide in snow pit samples do not support the importance of snowpack bromine emissions over the Antarctic Plateau. To evaluate the overall importance of the bromine chemistry over East Antarctica, BrO simulations were also discussed with respect data derived from GOME-2 satellite observations over Antarctica.

1. Introduction

The understanding of emissions and atmospheric fate of sea-salt aerosol at high latitudes is important for several reasons. First, sea-salt aerosol emitted from open ocean represents a potential large source of halogens [Sander *et al.*, 2003] that if activated plays an important role on the reactivity of the atmosphere over these regions (see Simpson *et al.* [2007] and Abbatt *et al.* [2012] for reviews as well as Yang *et al.* [2005], Parrella *et al.* [2012], and Long *et al.* [2014] for instance). Second, related to the presence of sea ice, emissions from blowing snow [Yang *et al.*, 2008; Jones *et al.*, 2009] or other sea-ice-related processes (e.g., frost flowers [Wagenbach *et al.*, 1998a; Rankin *et al.*, 2000]) could represent a significant (possibly dominant) sea-salt aerosol source with respect to the common sea-salt emissions from open ocean in these regions. That offers the possibility to reconstruct an important proxy of the past climate, namely, the sea ice extent [Rankin *et al.*, 2002; Abram *et al.*, 2013], through the study of sea-salt ice core records.

With the aim to test the possibility of using sea-salt ice core records to derive past sea ice extent, Levine *et al.* [2014] developed a chemistry transport model, p-TOMCAT (parallelized-Tropospheric Offline Model of Chemistry and Transport), that includes open ocean and blowing-snow sources. The model was tested against atmospheric sea-salt observations available at the central Antarctic sites of Concordia and Kohnen and the coastal sites of Neumayer and Palmer, confirming the importance of sea-ice-related sea-salt emissions in winter at both coastal and central Antarctica.

Whereas the importance of sea salt as a source of bromine species over the vast region of middle to high southern latitudes is now well established [Yang *et al.*, 2005, 2010], there are large uncertainties in quantifying bromine release from sea-salt aerosol [Sander *et al.*, 2003; Breider *et al.*, 2010; Long *et al.*, 2014]. Most bromine chemistry models used observed sea-salt depletion of bromide relative to sodium (or chloride) with respect

to seawater composition to describe the release of bromine from sea-salt aerosol. However, data are only available northward of 55°S [see *Sander et al.*, 2003, and references therein]. Model simulations are generally validated by comparing with either the few available near-surface BrO measurements or the tropospheric BrO vertical column derived from satellite observations [*Theys et al.*, 2011]. The role of the photochemistry within the snowpack present over polar ice sheets is suspected [*Thomas et al.*, 2011; *Dibb et al.*, 2010] but not yet discussed for Antarctica.

We here report on multiple-year atmospheric observations of sea salt at two sites located in East Antarctica, Dumont d'Urville (DDU) at the coast and Concordia on the high plateau. These bulk aerosol data are complemented by the study of size-segregated aerosol composition to quantify the contribution of sea-ice-sourced versus open-ocean-sourced emissions. The aerosol (bulk and size-segregated sampling) records at DDU also document, for the first time in Antarctica, the depletion of bromide relative to sodium over the course of the year. Gaseous inorganic bromine species were also sampled year-round for 8 years at DDU and 5 years at Concordia. Finally, the bromide snow pack content at Concordia was documented to evaluate the contribution of bromine snow emissions to the atmospheric boundary layer there in summer. These near-surface data on sea-salt aerosol and gaseous inorganic bromine, together with satellite observations of BrO, were compared to off-line chemistry transport model simulations to evaluate the importance of bromine chemistry in East Antarctica.

2. Sites and Methods

Inorganic bromine was investigated in aerosol and gas atmospheric samples collected in East Antarctica at the continental site of Concordia (75°06'S, 123°33'E, 3233 m above sea level) and the coastal site of Dumont D'Urville (66°40'S, 140°01'E, at sea level) (Figure 1). In water-extracted samples, anions including chloride, nitrate, sulfate, methanesulfonate (denoted MS^-), and bromide were determined by using ion chromatography (IC) equipped with a 1 mL sample loop. Cations including sodium, ammonium, potassium, calcium, and magnesium were determined using a CS12 separator column. Working IC conditions are detailed in *Minikin et al.* [1998] and *Wagenbach et al.* [1998a]. The IC analyses of anions in atmospheric samples were done using an AS11 separator column with which bromide is eluted just before nitrate (retention time of 8.7 min instead of 8.8 min for nitrate). Such a short time interval renders difficult accurate measurements of bromide in samples containing a relative large abundance of nitrate compared to bromide (see further discussions in sections 2.1 and 2.3). In this paper, atmospheric bromide concentrations are reported in $ng\ m^{-3}$ STP (standard temperature and pressure conditions of 298 K and 1013 hPa), a mixing ratio of 24.4 pptv corresponding to a concentration of $1\ nmol\ m^{-3}$ STP (i.e., $80\ ng\ m^{-3}$ STP).

2.1. Aerosol Sampling and Measurements

Aerosol samplings were conducted at DDU and Concordia in the framework of the French environmental observation service CESOA (Etude du cycle atmosphérique du Soufre en liaison avec le climat aux moyennes et hautes latitudes Sud, <http://www-igge.obs.ujf-grenoble.fr/CESOA/spip.php?rubrique3>) dedicated to the study of the sulfur cycle at middle and high southern latitudes.

At DDU, bulk aerosol samples were continuously collected on Gelman Zefluor (47 mm diameter, 0.5 mm pore size) filters at a flow rate of $1.7\ m^3\ h^{-1}$. A typical sampling interval of 1 day was applied from the end of October to the beginning of April and 2 days during the remaining winter months, respectively (i.e., 260 samples per year from 2004 to 2013). Filters were extracted in 1 mL of methanol (to aid wetting of the filter) plus 9 mL of ultrapure water. No detectable amount of bromide was found in blanks of the filter extraction procedure and the detection limit is only related to the detection limit of the IC ($0.05\ ng\ g^{-1}$). With values ranging from $0.01\ ng\ m^{-3}$ to more than $10\ ng\ m^{-3}$ in samples containing large amount of sea salt (sodium concentrations exceeding $2000\ ng\ m^{-3}$), bromide concentrations are well above detection limit ($0.01\ ng\ m^{-3}$ in winter and $0.02\ ng\ m^{-3}$ in summer). As discussed above, under working conditions applied to the AS11 separator column, bromide is eluted only 6 s before nitrate. Although Teflon filters do not retain efficiently HNO_3 [see *Wagenbach et al.*, 1998b], at DDU a large fraction of total atmospheric nitrate is trapped in the aerosol filters which, as discussed in section 2.2, are very alkaline in summer due to high ammonia emissions caused by the presence of a large penguin colony at that site [*Legrand et al.*, 1998]. Bromide and nitrate concentrations are smaller in winter than in summer, but due to an earlier recovery of summer values for nitrate ($80\ ng\ m^{-3}$ in November instead of $12\ ng\ m^{-3}$ in May on average over the years 2004–2013, not shown) than for bromide

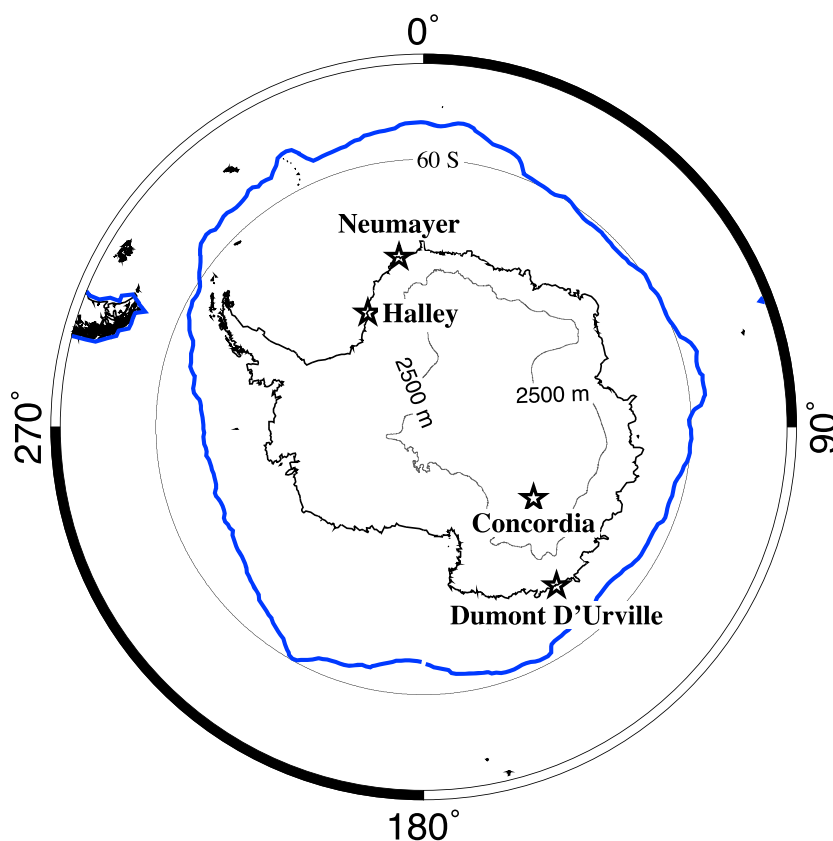


Figure 1. Map of Antarctica showing the locations of Dumont D'Urville, Concordia, Halley, and Neumayer stations. The blue line refers to the mean location of the sea ice edge end of winter (August) over the period 1981–2012 (NOAA_OI_SST_V2 data provided by the NOAA/OAR/ESRL PSD, Boulder, Colorado, USA, <http://www.esrl.noaa.gov/psd>).

(maximum of 5 ng m^{-3} in January, see below), the relative abundance of bromide with respect to nitrate drops in November compared to the rest of the year (bromide to nitrate mass-based ratio of 0.02 compared to a maximum of 0.16 in May). The determination of bromide becoming less accurate in samples containing a relatively large concentration of nitrate, on a total of 2600 bromide values, around 500 values in which the mass-based ratio of bromide to nitrate were smaller than 0.02 were considered as too uncertain to calculate the bromide to sodium mass-based ratio. The 2004–2013 time series of bromide in aerosol is presented in Figure 2 in 10 day binned averages. The acidity (or alkalinity) of samples (not measured) was evaluated by checking the ionic balance between dominant anions and cations with concentrations expressed in microequivalents per liter, $\mu\text{Eq L}^{-1}$ (positive and negative values corresponding to acidic and alkaline samples, respectively):

$$[\text{H}^+] = ([\text{Cl}^-] + [\text{NO}_3^-] + [\text{SO}_4^{2-}] + [\text{CH}_3\text{SO}_3^-] + [\text{C}_2\text{O}_4^{2-}]) - ([\text{Na}^+] + [\text{K}^+] + [\text{Mg}^{2+}] + [\text{Ca}^{2+}] + [\text{NH}_4^+]) \quad (1)$$

In addition to multiple-year bulk aerosol samplings, a year-round study of size-segregated aerosol composition has been carried out at DDU on 47 discontinuous samplings done from January 1999 to August 2001 by using a small deposit area impactor, similar to the one developed by *Maenhaut et al.* [1996], and equipped with a $20 \mu\text{m}$ cutoff diameter inlet. Typically, eight runs were done during each of the three summers (from November to February) and three runs each winter. The 16 runs done in 2001 were only analyzed for anions. A flow rate of $0.84 \text{ m}^3 \text{ h}^{-1}$ was applied with a sampling interval of 1 to 3 days in summer, 4 to 7 days in winter. As detailed in *Jourdain and Legrand* [2002], the impactor has been run with 11 stages whose cutoff diameters range from 0.08 to $7.7 \mu\text{m}$. Using a 10 mL extraction volume and given the air sampled volume, the bromide detection limit was as low as 0.01 ng m^{-3} in summer and 0.005 ng m^{-3} in winter. With that, even with a few ng m^{-3} of sodium collected on the bottom stages of the impactor, bromide can be detected. In most of the cases, bromide was found above the detection limit on all stages collecting particles with diameter larger

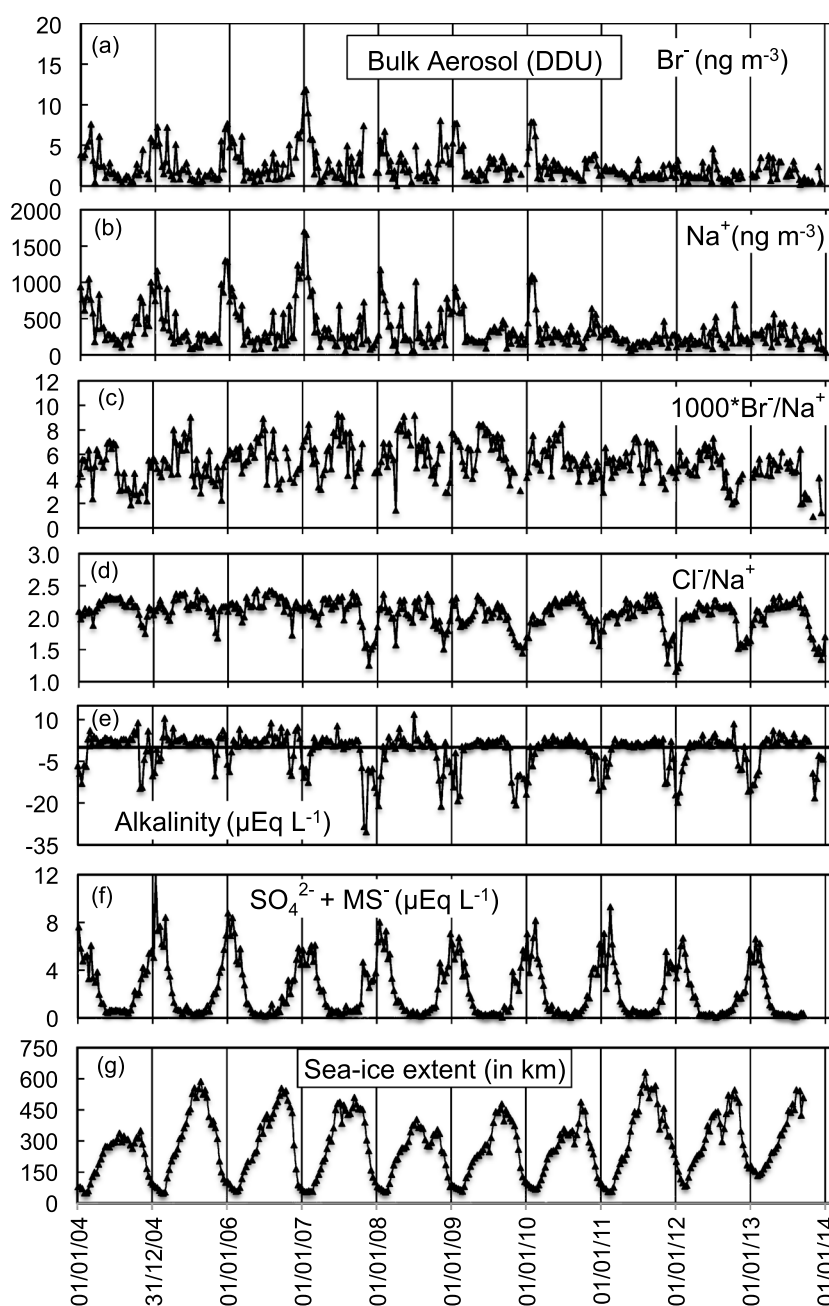


Figure 2. Ten day averaged concentrations of (a) bromide and (b) sodium, (c) bromide to sodium, and (d) chloride to sodium mass-based ratios, (e) acidity or alkalinity (see equation (1)), (f) sum of acidic sulfur aerosol components (non-sea-salt sulfate and methanesulfonate) in bulk aerosol continuously collected at DDU from January 2004 to December 2013. (g) Sea ice extent (mean distance between the DDU coastline and the ocean with less than 15% of ice within the 130–150°E sector).

than $0.25 \mu\text{m}$. In 14 of the 47 runs, not enough sea salt was collected (total sodium and chloride concentrations as low as $33\text{--}77 \text{ ng m}^{-3}$ and $14\text{--}42 \text{ ng m}^{-3}$, respectively) to permit accurate detection of bromide. As acidic gaseous compounds present in the sampled air like nitric acid have a quite limited access to particles deposited on the substrate, the observed concentrations of nitrate collected on the impactor are a factor 2 to 5 smaller than those observed on the corresponding bulk aerosol filters. The previously discussed difficulty to measure bromide in samples having a bromide to nitrate mass-based ratio lower than 0.02 was therefore very rare and, when it did occur, was limited to submicron stages that are of less importance when evaluating bromide depletion in sea-salt aerosol (see section 3.2).

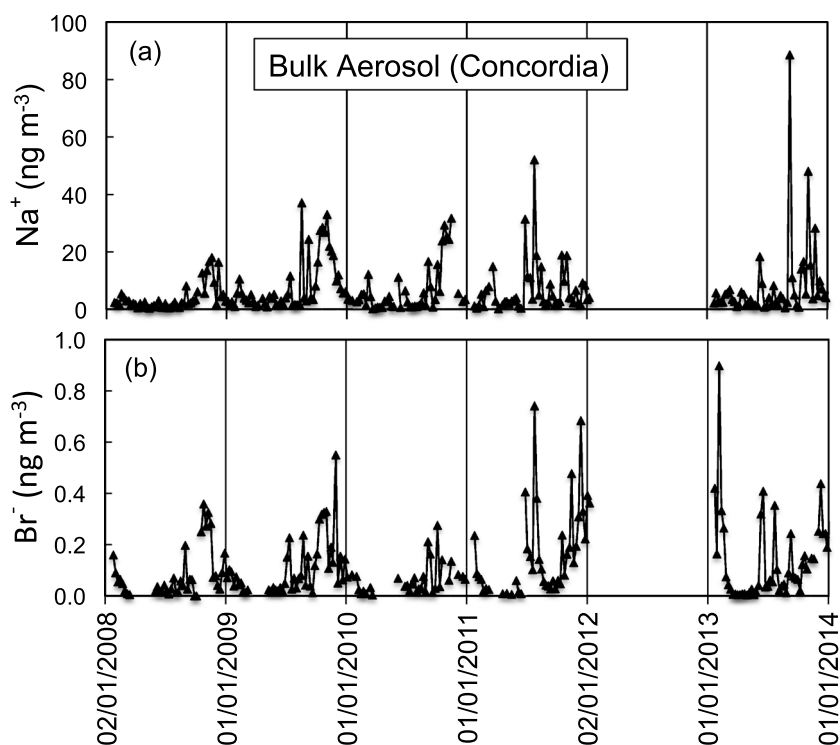


Figure 3. Bulk aerosol concentrations of (a) sodium and (b) bromide (weekly sampling) at Concordia since early 2008.

Year-round composition of aerosol was examined on samplings made at Concordia since 2006. Aerosol was continuously sampled at a flow rate of $1.1 \text{ m}^3 \text{ min}^{-1}$ on circular quartz filters (Gelman Pallflex Tissuquartz 2500QAT-UP) with 15 cm diameter (filter holder from Digitel). A piece of each filter (10 cm^2 of a total surface of 150 cm^2) was extracted with 10 mL of ultra pure Milli-Q water. Given the weekly sampling time, a far larger air volume was sampled (8000 m^3 compared to $35\text{--}70 \text{ m}^3$ at DDU) permitting the determination of bromide as low as 0.001 ng m^{-3} . Note that quartz filter used here does not trap efficiently nitric acid and the above-discussed overlap between nitrate and bromide was less important than at bulk aerosol collected at DDU. As seen in Figure 3, concentrations range from detection limit (0.001 ng m^{-3}) to 0.4 ng m^{-3} (mean value of 0.1 ng m^{-3}). A study of the size-segregated aerosol composition was carried out at Concordia, but even with a sampling interval of 2 weeks applied with a flow rate of $0.84 \text{ m}^3 \text{ h}^{-1}$, the detection of bromide remained difficult to derive relevant information on the size-segregated bromide composition. That is mainly due to the low sodium concentration at that site (reaching at the best only a few ng m^{-3} on the stage collecting particles of $\sim 1 \mu\text{m}$ diameter).

2.2. Gaseous Inorganic Bromine Sampling and Measurements

Measurements of soluble bromide trapped in mist chambers [Ridley *et al.*, 2003; Dibb *et al.*, 2010; Liao *et al.*, 2012b] and denuder tubes [Sturges *et al.*, 1993; Li *et al.*, 1994] were previously used in polar regions, providing relevant information on the active bromine chemistry. At DDU, a gas sampling line of three Na_2CO_3 -coated annular denuder tubes placed in series [Jourdain and Legrand, 2002; Legrand *et al.*, 2012] was run with a flow rate of $0.6 \text{ m}^3 \text{ h}^{-1}$ (405 runs done from end of January 2006 to end of December 2013, Figure 4a). The coating was made with a solution of Na_2CO_3 at 10^{-2} M (50% ultrapure water, 50% high-performance liquid chromatography methanol). At each denuder tube series, one tube was used as a blank to control the quality of the preparation procedure and the effect of storage of tubes before their use (a day or a few days later). No detectable amount of bromide was found (less than 0.05 ng g^{-1}). Each tube sampling was extracted in 5 mL of ultrapure water. From January 2009 to December 2010, a sampling interval of 10 h and 30 h was applied in summer and winter, respectively. Since beginning of 2011, the sampling is more continuous and the sampling time was increased to 6 days in both winter and summer (Figure 4a). With sampling interval of 10 h in summer, the blank value corresponds to an atmospheric concentration of 0.04 ng m^{-3} . In winter,

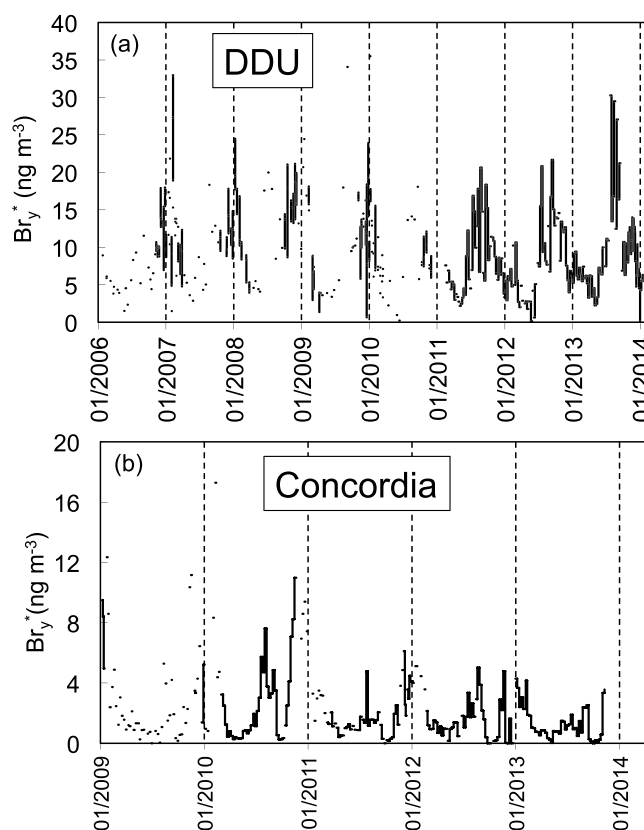


Figure 4. Year-round records of inorganic gaseous bromine (Br_y^* , see equation (2)) sampled on denuder tubes at (a) DDU from 2006 to 2014 and (b) Concordia from 2009 to 2013.

the longer sampling interval (30 h) leads to smaller values (0.015 ng m^{-3}). The collection efficiency of the first tube (defined as the mass trapped on the front tube divided by the sum of masses in the three tubes) was on average $65 \pm 10\%$, $85 \pm 5\%$ of the sum of masses having been trapped on the front tube and the tube placed behind. Note that with bromide to nitrate mass-based ratios close to 0.2 in summer and 1 or 2 in winter in denuder tube extracts, the interference between the two anions is far less important than in the case of aerosol extracts.

Bromide present in water extracts from denuder tubes cannot distinguish HBr from other brominated species like HOBr, Br_2 , BrNO_2 , and BrONO_2 that were likely also collected on the denuder tubes [Li *et al.*, 1994]. Only BrO is thought to be weakly retained during denuder sampling [Sturges *et al.*, 1993]. More recently, Liao *et al.* [2012b] characterized the response of mist chamber for HBr, HOBr, BrO, and Br_2 by using chemical ionization mass spectrometer. They demonstrated that whereas the four species are efficiently trapped in water, the molar ratios of detected bromide to Br_2 and to BrO was 0.45 and 0.4, respectively. From that it can be assumed that in the presence of these four species, bromide in mist chamber corresponds to $[\text{HBr}] + [\text{HOBr}] + 0.9[\text{Br}_2] + 0.4[\text{BrO}]$. Liao *et al.* [2012b] concluded that, in the mist chamber, the Br_2 hydrolysis products are Br^- and HOBr, the latter being not converted to bromide at the time scale of measurements (5 min). For BrO the reaction converting 40% of BrO to bromide is not known. It is difficult to evaluate if the missed fraction of HOBr or BrO is trapped or not when using two mist chambers in series run during 2 to 4 h.

On the basis of preceding discussions and given the use of two mist chamber in series or three denuder in series, we have assumed that the determination of bromide in water extract (denoted Br_y^*) would correspond to the sum of all inorganic gaseous brominated species ($[\text{Br}_y] = [\text{HBr}] + [\text{HOBr}] + 2[\text{Br}_2] + [\text{BrO}] + [\text{BrNO}_2] + [\text{BrONO}_2] + [\text{Br}]$) or to $[\text{Br}_y^*] \cong [\text{Br}_y] - 1.1[\text{Br}_2] - 0.6[\text{BrO}] = [\text{HBr}] + [\text{HOBr}] + 0.9[\text{Br}_2] + 0.4[\text{BrO}] + [\text{BrNO}_2] + [\text{BrONO}_2] + [\text{Br}]$ (2)

Gas phase samplings were also done at DDU until January 2010 by using two mist chambers placed in series downstream from a Teflon Millipore Type FALP (37 mm diameter) filter with an airflow rate of $0.36 \text{ m}^3 \text{ h}^{-1}$. Blanks were done at least once per week showing no detectable amount of bromide (less than 0.05 ng g^{-1}).

Table 1. Comparison of Monthly Mean Inorganic Gaseous Bromine Concentrations (Br_{y^*} , See Equation (2)) Derived From Mist Chamber (1360 Samplings) and Denuder Tube (250 Samplings) Samplings Done at DDU Between January 2006 and January 2010^a

Months	Br_{y^*} (in $ng\ m^{-3}$) Mist Chambers	Br_{y^*} (in $ng\ m^{-3}$) Denuder Tubes	Acidity (Alkalinity) of Bulk Aerosol ($\mu Eq\ L^{-1}$)
Jan	10.2 ± 1.9	11.9 ± 6.3	-8.5
Feb	6.9 ± 0.3	11.3 ± 4.0	-4.5
Mar	5.6 ± 1.0	6.6 ± 1.7	+0.7
Apr	6.0 ± 1.2	4.2 ± 1.0	+2.0
May	4.4 ± 1.9	3.4 ± 1.0	+2.3
Jun	5.8 ± 2.6	6.8 ± 4.8	+1.8
Jul	7.3 ± 4.0	10.0 ± 5.1	+2.4
Aug	9.4 ± 3.9	9.9 ± 6.3	+2.2
Sep	8.2 ± 2.5	13.0 ± 6.5	+2.6
Oct	8.3 ± 2.0	9.1 ± 2.9	0
Nov	9.4 ± 2.8	11.5 ± 6.9	-8.0
Dec	10.2 ± 3.8	11.0 ± 3.7	-3.6

^aStandard deviations refer to the variability of mixing ratios observed from individual samples collected each month. The last column refers to the monthly means acidity (alkalinity) of bulk aerosol sampled at DDU (see equation (1)).

These values remain insignificant with respect to atmospheric levels, even in winter. 1360 runs of mist chambers were done from November 2005 to the end of January 2010. Monthly mean Br_{y^*} concentrations derived from samplings from mist chambers are compared to those from denuder tubes (Table 1). In spite of a significant day-to-day variability, the two monthly mean data sets indicate similar absolute values and seasonal trend. It is important to note that in spite of the strong alkaline character of bulk aerosol in summer, particularly in November and January (see Figure 2e and Table 1) when penguin activities reach a maximum [Legrand *et al.*, 1998], there is no evidence that acidic compounds like HBr or HOBr were trapped on the corresponding front filters of mist chambers. Indeed, no decrease of mist chamber values with respect to denuder tube ones can be observed during these two months, the largest departure being observed in September and February.

Finally, 261 denuder tube runs were done at Concordia between January 2009 and March 2014 (Figure 4b). Over the first year, a sampling interval of 2 to 3 days was applied in summer and winter, respectively. From 2010 to 2013 the sampling became more continuous and the sampling time was increased to 6 days both for winter and summer (Figure 4b). With sampling interval of 3 days in summer, the blank values correspond to atmospheric concentration of $0.01\ ng\ m^{-3}$. With a bromide to nitrate mass-based ratio close to 0.05 in summer and 1 in winter, nitrate does not significantly interfere with bromide during analyses.

2.3. Snow Samples

At Concordia, a snow pit was dug 9 January 2012, 3 km from the station and sampled down to 110 cm depth. All samples collected within the upper 10 cm of snow and a few samples collected between 15 cm and 60 cm depth were analyzed for bromide. As seen in Table 2, the samples contain relatively large amount of nitrate and their

Table 2. Bromide and Nitrate Concentrations in Snow Samples Collected in a Snow Pit Dug at Concordia in January 2012

Depth (cm)	Nitrate ($ng\ g^{-1}$)	Bromide ($ng\ g^{-1}$)	Snow Density ($kg\ m^{-3}$) ^a
0.3 – 2.0	82	0.100	0.26
2–4	76	0.08	0.295
4–6	31	0.04	0.315
6–8	25	0.04	0.33
8–10	23	0.007	0.35
10–12	23	0.01	0.35–0.375
14–16	32		
22–24	35		
40–42	9		
57–59	7	0.02	

^aSnow densities are from Gallet *et al.* [2011].

analyses were not possible using working conditions applied to atmospheric samples (see section 2.1). Here we used a concentrator column (sample volume of 5 mL) and an AS18 separator column with which nitrate does not interfere with bromide. It was, however, necessary to adjust the pH of samples by adding HCl (2×10^{-3} M) to reduce the interference between bromide and bicarbonate which is present in samples as the result of CO_2 solubilization. Under these working conditions, a detection limit as low as $0.007\ ng\ g^{-1}$ is achieved.

2.4. GOME-2 Tropospheric BrO Vertical Columns

To evaluate the role of bromine chemistry throughout the entire troposphere, in addition to data gained nearby the ground, we also examine data derived from satellite observations. The second Global Ozone Monitoring Instrument (GOME-2) is a nadir-looking UV-visible spectrometer measuring the solar radiation backscattered by the atmosphere and reflected by the Earth in the 240–790 nm wavelength interval and with a spectral resolution of 0.2–0.5 nm [Munro *et al.*, 2006]. It is in a Sun-synchronous polar orbit on board the Meteorological Operational satellite-A (MetOp-A), launched in October 2006, and has an Equator crossing time of 09:30 local time on the descending node. The ground pixel size is typically of about 80 km × 40 km and GOME-2 provides nearly complete coverage of polar regions every day. The tropospheric BrO columns are retrieved following the method described in Theys *et al.* [2011], which consists of three steps: (1) the measured spectra are analyzed for BrO using differential optical absorption spectroscopy (DOAS), (2) the contribution from the stratosphere is estimated and subtracted from the results, and (3) radiative transfer calculations which account for changes in surface reflectivity, observation geometry and clouds are performed, to convert the measured quantity into a tropospheric column.

2.5. Model Descriptions and Simulations

2.5.1. Three-Dimensional Model for Sea-Salt Aerosol and Br₂ Species

Sea-salt model simulations were done using a global chemistry 3-D transport model p-TOMCAT. It is driven by winds, temperatures, water vapors based on 6-hourly European Centre for Medium-Range Weather Forecast interim data, with monthly fractional sea ice coverage and sea surface temperature data from the Hadley Centre Sea Ice and Sea Surface Temperature (HadISST) data set [Rayner *et al.*, 2003]. A model horizontal resolution of 2.8° × 2.8° was used with 31 vertical layers from the surface to 10 hPa at the top layer.

The model includes tropospheric bromine chemistry based on the previous works of Yang *et al.* [2005, 2010] with bromine sources from both short-lived bromocarbons and sea-salt bromine depletion. The halocarbon emissions are based on the original work (scenario 5) of Warwick *et al.* [2006], except for emissions of CH₂Br₂, which were updated to 57 Gg/yr [Yang *et al.*, 2014]. Sea-salt bromine flux was estimated using depletion factors (denoted DF) which represents the fraction of bromine having been lost from aerosol to the gas phase and being equal to $1 - [\text{Br}^-/\text{Na}^+]_{\text{aerosol}}/[\text{Br}^-/\text{Na}^+]_{\text{seawater}}$. To represent seasonal change in bromine release from sea salt in the Southern Ocean at latitudes higher than 30°S, the seasonal change of DF was implemented. In this study, we updated DF values for latitudes higher than 60°S based on data obtained at DDU (see Table 3 and discussions in section 3.2), while for the 50°S–60°S latitude band, DF values observed at Macquarie Island (55°S, 159°E) were used [Ayers *et al.*, 1999]. For latitudes north of 30°S, a size-dependent DF scheme from Breider *et al.* [2010, supplementary] was used (nonseasonal variation), which is in general ~2 times higher than that of the DF scheme used in simulations from Yang *et al.* [2008, 2010]. With respect to the previous works from Yang *et al.* [2005, 2010], the dry deposition of HBr, HOBr, and BrONO₂ over snow and ice was enhanced (see further discussions in section 3.3).

Levine *et al.* [2014] have successfully introduced a process-based detailed sea-salt aerosol scheme, including production, transport, and wet and dry depositions of sea salt to the p-TOMCAT model. The sea-salt parameterization was based on the work from Reader and McFarlane [2003]. The open ocean sea-salt production was updated following Caffrey *et al.* [2006] by choosing the maximum flux of Gong [2003] and Smith *et al.* [1993] for wind speeds higher than 9 m s⁻¹, for wind speed lower than 9 m s⁻¹ the flux from Gong [2003] was applied. Sea-salt production from sea ice followed the original work of Yang *et al.* [2008]. The key parameter, snow salinity, was updated based on recent investigations made during a wintertime cruise of the Polarstern (June–August 2013) in the frame of the BLOWSEA project conducted by the British Antarctic Survey. The top 10 cm of snow plus blown samples gave an averaged surface snow salinity of ~0.3 practical salinity unit (M. Frey, personal communication, 2015), which is more than 10 times smaller than the column mean value used in the original parameterization. In all simulations, following Levine *et al.* [2014], an averaged snow age of 36 h was assumed. We also improved the model precipitation field by introducing monthly precipitation ratios between climatology (Monthly Global Precipitation Climatology Project) [Adler *et al.*, 2003] and modeled multiyear mean. The precalculated ratio for each grid box was used in further model integration with the aim of forcing its total precipitation close to its climatology. This method appeared to be a better way to correct large bias in the model precipitation field than that using manual correction as done in Levine *et al.* [2014].

Table 3. Bromide to Sodium Mass-Based Ratio (Multiplied by 1000) in Bulk Aerosol Filters Continuously Collected at DDU From 2004 to 2013 and on a Few Impactor Runs^a

Months	1000 Br ⁻ /Na ⁺ in Bulk Aerosol	1000 Br ⁻ /Na ⁺ on Impactor (Number of Runs)	1000 Br ⁻ /Na ⁺ Sea-Salt Reference	DF in Bulk Aerosol
Jan	5.55 (4.94)	4.3 ± 0.7 (3 runs)	6.25	0.11 (0.21)
Feb	5.72 (5.14)	4.6 ± 0.3 (2 runs)	6.25	0.085 (0.18)
Mar	5.04 (4.60)	No run	6.25	0.194
Apr	5.71 (5.28)	No run	6.9	0.17
May	6.38 (5.59)	No run	7.5	0.15
Jun	7.22 (6.65)	6.0 (1 run)	7.5	0.04
Jul	5.87 (5.34)	5.0 (1 run)	7.5	0.22
Aug	5.39 (5.23)	No run	7.5	0.28
Sep	4.54 (4.28)	No run	7.5	0.39
Oct	4.35 (3.78)	No run	7.5	0.42 (0.49)
Nov	3.88 (3.17)	3.4 ± 0.1 (2 runs)	6.25	0.38 (0.49)
Dec	4.20 (4.35)	4.15 ± 0.6 (7 runs)	6.25	0.33 (0.31)

^aThe last column refers to the bromide depletion factor (DF, see section 3.2) calculated using sodium as the sea-salt reference species and the bromide to sodium mass-based ratio in seawater. The mass-based ratio in sea-salt aerosol was assumed to be equal in summer to the one of seawater ($6.25 \cdot 10^{-3}$) and 20% higher in winter due to precipitation of mirabilite at that season (see section 3.1). Mass-based bromide to sodium ratios and DF values in bulk aerosol reported under parenthesis refer to mean values calculated for 2010–2013 over which an unusual presence of sea ice offshore the site in summer took place (see section 3.1).

A 5 year period of 2008–2012 was run with monthly output of tagged sea salt from both open ocean and sea ice zone, and bromine compounds (BrO, HBr, HOBr, Br₂, BrNO₂, BrONO₂, and atomic Br). For years 2008 and 2009, an output frequency interval of 2 h was used to derive satellite overpass time BrO for a direct comparison with GOME-2 BrO data.

2.5.2. One-Dimensional Model for Snow Br_y Emissions

A 1-D box model was used to investigate the possible role of snow emissions on the observed mixing ratio of Br_y at Concordia. The vertical transport of the 1-D model was represented using vertical distribution of turbulent diffusion coefficients (K_z) calculated by the regional atmospheric MAR model (Modèle Atmosphérique Régional). More details of MAR and of its reliability at Concordia are given in *Gallée et al.* [2015]. Similarly to calculations performed by *Legrand et al.* [2014], we used the MAR data obtained with a horizontal resolution of 20 km centered at Concordia, a vertical resolution of 0.9 m for the height of up to 23 m above the surface decreasing upward to about 50 m at the height of 500 m and to ~ 1800 m at the top level of ~ 24 km. For the 1-D model, the K_z values were linearly interpolated to the vertical 1-D grid which was 0.1 m from the surface to 5 m, 0.2 m from 5 to 7 m, 0.5 m from 7 to 10 m, around 1 m from 10 to 20 m, and then increases up to 120 m at 1200 m, the top height of the 1-D model. Note that the planetary boundary layer height, defined by MAR as the height where the turbulent kinetic energy decreases below the value at the lowest layer of the model, was always lower than the top layer of the 1-D model.

3. Results and Discussions

3.1. Observed and Simulated Sea-Salt Concentrations: Contribution of Open-Ocean-Related Versus Sea-Ice-Related Processes

3.1.1. The Case of DDU

As seen in Figure 2b, in general, the year-round sodium record at DDU exhibits a summer maximum. As already discussed by *Wagenbach et al.* [1998a] such a seasonal pattern is reversed compared to those observed at other coastal Antarctic sites where the largest concentrations occur in winter. This finding pointed out the sea ice as an efficient source of sea-salt aerosol in winter. The outstanding summer maximum of sea-salt concentrations only detected at DDU is related to the particularity of this site, located on a small island with open ocean immediately around from December to February. This particularity of DDU was confirmed by an absence of summer sodium maximum observed in January 1995 when exceptionally severe summer sea ice conditions had prevailed at the site [*Jourdain and Legrand, 2002*]. As seen in Figure 2g, this phenomenon occurred again during more recent summers (2011/2012, and 2012/2013) for which summer sea ice conditions were severe (the area of ocean containing more than 15% of ice having extended up to 50 km offshore DDU). In Figure 2g,

original sea ice extent data from the National Snow and Ice Data Center (<http://nsidc.org/>) were resampled with a longitudinal resolution of 10° [Weller *et al.*, 2011]. It should be emphasized that this summer sea ice is soft and does not permit emissions of sea-salt aerosol, unlike the case in winter. In contrary, its presence offshore DDU leads to an accumulation of sea ice pack between the numerous small islands of the Archipelago. This likely limits the effect of breaking waves around the site in emitting locally large particles. It should be emphasized that this change of sea ice conditions in summer offshore DDU, which would slightly weaken the open ocean source, cannot be captured by the model.

As seen in Figures 5c and 5e, the model overestimates sodium concentrations observed at DDU by a factor of ~ 2 in summer and ~ 3 in winter. This comparison between observations and simulations was done by considering in the model NaCl particles having a dry diameter smaller than $10\ \mu\text{m}$. Given relative humidity encountered at DDU when marine air masses rich in sea-salt aerosol reach the site, typically 60% to 90%, a sea-salt particle of $10\ \mu\text{m}$ dry diameter would have an ambient air diameter twice larger (around $20\ \mu\text{m}$). Whereas this value is close to the cut off of the impactor deployed at DDU in 2000 and 2001 (see section 2.1), data gained with the impactor are too sparse to be used in the comparison reported in Figure 5 where we used data derived from bulk filters. It has to be kept in mind that as discussed in section 3.2, sodium data derived from bulk filter sampling are on average 50% higher than those derived from simultaneous sampling with the impactor, likely due to the larger cutoff size of bulk aerosol filter sampling with respect to the one the impactor. Thus, the departure between simulations and observations may be even larger than depicted in Figure 5.

In general, the p-TOMCAT model was shown to underestimate sodium concentrations at marine sites, for example, by a factor of ~ 2 at both the coastal Antarctic site of Neumayer and at Cape Grim (not shown). A possible reason for the particular case of DDU characterized by an overestimate of sea-salt concentrations by the model by more than a factor of 2 may be due the fact that the site experiences strong katabatic winds coming down from the ice cap situated south of DDU that brings sea-salt poor air from the Antarctic Plateau. Indeed, as discussed by König-Langlo *et al.* [1998], DDU experiences either air masses coming from inland Antarctica, purely marine air masses, or continental/marine mixed air masses with easterly winds due to arrival of low-pressure systems from the north. The effect of wind pattern on sea-salt concentrations at DDU is examined in Figures 6–8 for which the fractions of sampling time during which winds were blowing from the ocean (from 0 to 110°E , 270 to 360°E , denoted as Ocean and expressed in percent), the coastal glaciers (from 110 to 130°E) and the continent (from 130 to 270°E , denoted as Continent and expressed in percent) were calculated.

In winter, as seen in Figure 6 for winter 2012, sodium concentrations over days dominated by winds blowing from oceanic sectors ($290 \pm 228\ \text{ng m}^{-3}$ when more than 50% of time winds were blowing from the ocean) are larger than over days that experienced winds blowing from continental sectors ($125 \pm 83\ \text{ng m}^{-3}$ when more than 50% of time winds were blowing from the continent). On average, in winter winds blow over a similar fraction of time from the ocean (32%), the coastal glaciers (36%), and the continent (32%). A noticeable exception is winter 2011 during which the smallest sodium mean concentration is recorded ($170\ \text{ng m}^{-3}$ instead of $240\ \text{ng m}^{-3}$ over other winters, Figure 2b) in relation with less frequent winds blowing from oceanic sectors (20% instead of 33% over other winters) and more frequent winds blowing from the continent (50% instead of 30% over other winters). On average, in summer winds blow 37% of time from the ocean, 38% from the coastal glaciers, and 25% from the continent. Interestingly, at the beginning of the record (from 2004 to 2010), summers that were characterized by high sodium concentrations, experienced 40% of time winds blowing from the ocean and only 16% of time winds blowing from the continent as opposed to the summer 2012/2013 during which winds were blowing only 20% of time from the ocean and 60% from the continent. These wind conditions have certainly contributed, in addition to the severe sea ice conditions discussed above, to the absence of summer maximum at that time (Figure 2).

In contrast to wind conditions that are largely controlled by synoptic situation in winter, in summer the wind regime is also influenced at a very local scale by an anabatic phenomenon. The continental wind still blows in summer but sometimes strongly decreases or even ceases entirely as temperature rises over midday. As a result, an apparent “sea breeze” is sometimes observed with local wind direction changing from 110 to 160°E to North. The effect of changing wind direction on the sea-salt concentrations at DDU in summer is illustrated in Figure 7. Over the reported period of 24 days, the sampling time resolution was increased from

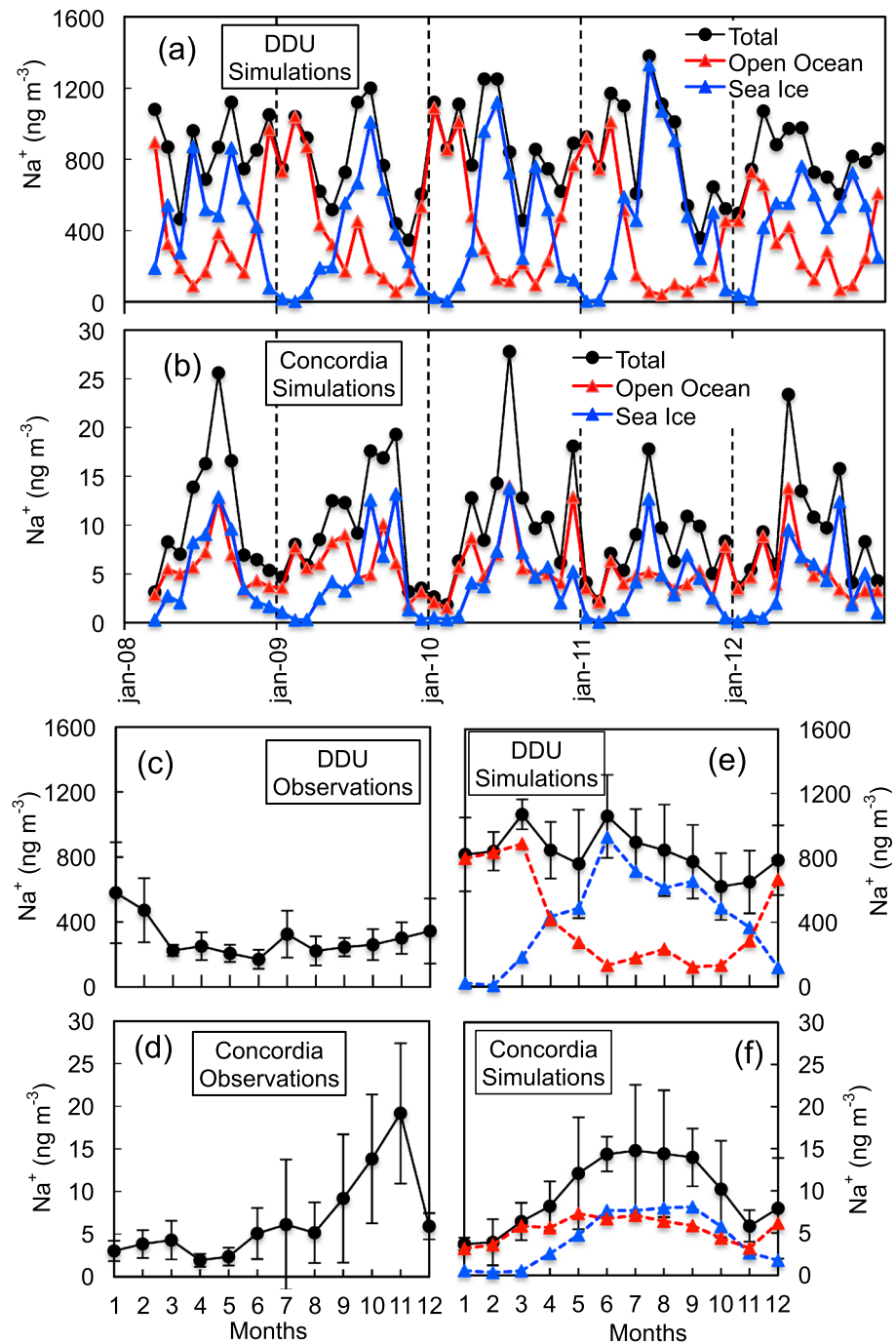


Figure 5. Simulated sodium concentrations at (a) DDU and (b) Concordia for 2008–2012. Monthly mean sodium concentrations observed (c) at DDU over 2008–2011 and (d) at Concordia over 2008–2011 and 2013 and simulated for 2008–2012 at (e) DDU and (f) Concordia.

a day to 6 hours to examine the effect of sea breeze. Over the period, several days experienced winds blowing from pure glacier sectors and from pure marine sectors. Over days with glacier sector winds (12, 13, 18, 19, 23, 25, and 28 December), the chloride concentrations remained some 5 times smaller than over days marked by marine sector winds (5, 15, 16, late 26, and 27 December). Between these two regimes, other days were in general marked by a change from glacier sector winds at night to marine sector winds in the afternoon (from 8 to 11, 14, 20 to 22, and 24 December). Over these sea breeze days a marked maximum of chloride can be observed in the afternoon or late afternoon.

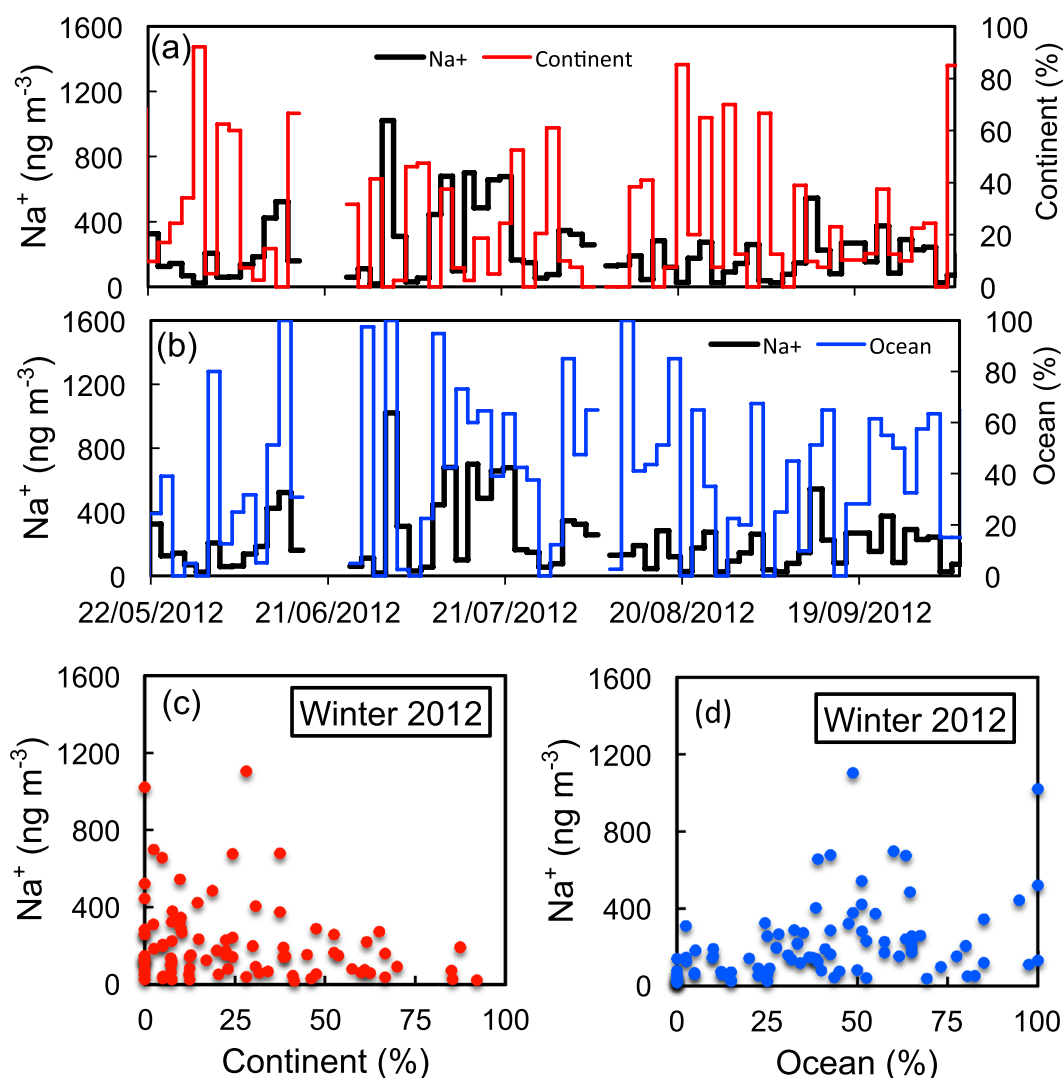


Figure 6. Sodium concentrations observed at DDU between 22 May and 4 October 2012 along with the fraction of sampling time during which winds were blowing (a) from the Continent and (b) from the ocean. (c and d) The same as Figures 6a and 6b but for the entire wintertime (from mid-April to mid-October 2012).

In Figure 8 we compare the effect of wind conditions on summer and winter sodium concentrations. It is seen that continental conditions more strongly decrease sodium concentrations in winter than in summer, possibly related to larger-scale phenomenon at that season. To evaluate the effect of winds blowing or not from oceanic sectors on the observed sodium concentrations, binned mean values (over 10% interval) were fitted using a polynomial function. From the best fits, that were obtained with a third-degree polynomial function, we estimated which sodium concentration is expected if the site would have been exposed permanently to winds blowing from the ocean and not influenced by the occurrence of glacier/continent winds. In summer, the sodium concentration is enhanced by a factor of 2 when these pure marine conditions are assumed instead of prevailing conditions (i.e., 35% of marine) using the best fit ($[Na^+] = -0.0013 \text{ Ocean}^3 + 0.1951 \text{ Ocean}^2 - 1.7392 \text{ Ocean} + 217$ with $R^2 = 0.88$). In winter, the sodium concentration is enhanced by a factor of 3 when these pure marine conditions are assumed instead of prevailing ones (i.e., 32% of marine) using the best fit ($[Na^+] = 0.0016 \text{ Ocean}^3 - 0.1933 \text{ Ocean}^2 + 8.3144 \text{ Ocean} + 65.5$ with $R^2 = 0.88$). Given the coarse horizontal resolution of the model (the size of the grid cell containing DDU is ~ 150 km in longitude, ~ 300 km in latitude), local small-scale meteorological phenomena like sea breeze and shallow katabatic flow could not be well represented by the model, which may affect the model-observation comparison. Therefore, the discrepancy between simulations and observations at DDU is likely

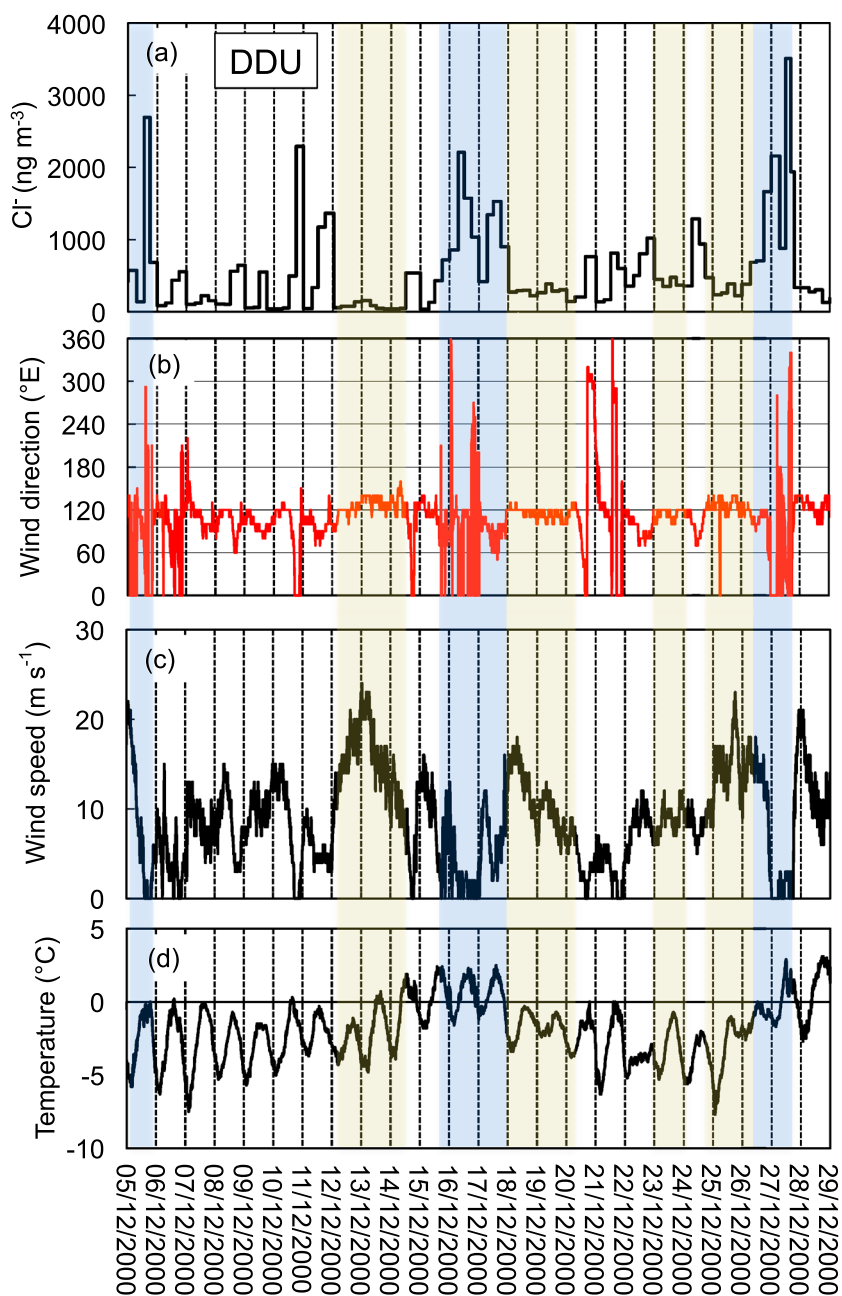


Figure 7. (a) Subdaily chloride concentrations observed at DDU in December 2000 along with (b, c) wind conditions and (d) temperatures. Winds blowing from 110°E to 130°E correspond to glacier sectors (colored in yellow), from 0°E to 110°E and 270°E to 360°E to marine sectors (colored in blue).

related to the particular conditions encountered at that site with dominant winds blowing from coastal glaciers and the Antarctic continent.

As seen in Figures 5d and 5f, the model experiments (with and without sea ice source) indicated that the winter sea-salt aerosol at DDU was dominated by sea ice emissions (68% of total from May to October). The overall importance of sea ice as a major source of sea-salt aerosol at coastal Antarctic sites in winter was first recognized by *Wagenbach et al.* [1998a] from the observation of a strong depletion of sulfate in atmospheric sea-salt aerosol due to precipitation of mirabilite ($\text{Na}_2\text{SO}_4 \cdot 10\text{H}_2\text{O}$) on the sea ice surface at that season. It was shown that the sea-salt atmospheric aerosol present at Neumayer site in winter (from May to October) is depleted in sulfate with a sulfate to sodium mass-based ratio of 0.07 (sulfate to chloride

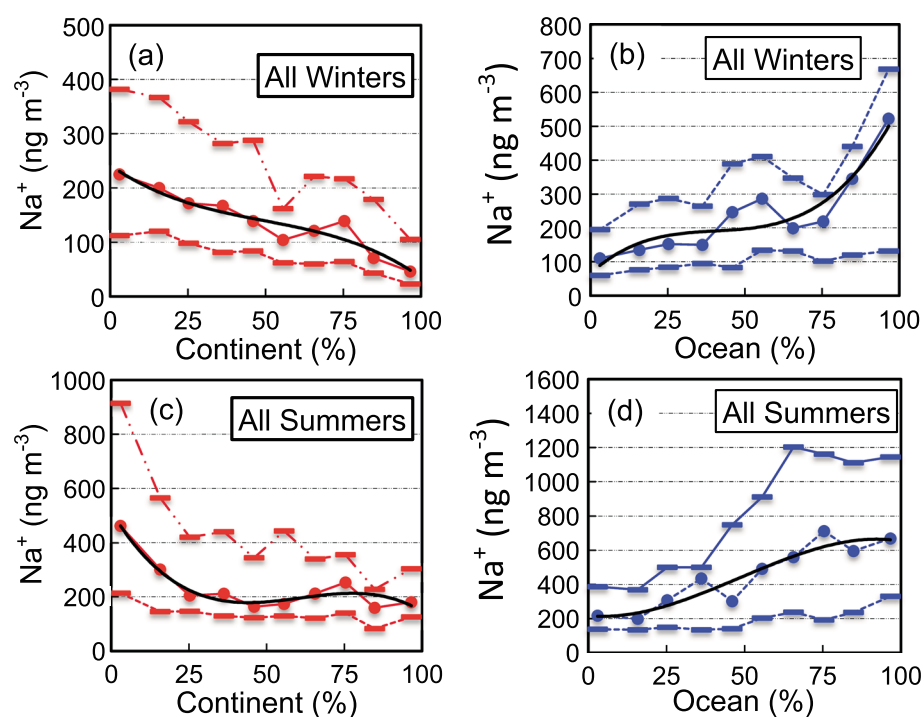


Figure 8. Winter sodium concentrations as a function of the sampling time during which winds were blowing (a) from the continent and (b) from the ocean (binned mean values for 10% interval). (c, d) The same as Figures 8a and 8b but for summer. The solid lines represent the best fits that were obtained with a third-degree polynomial function.

mass-based ratio of 0.04) with respect to the seawater composition (sulfate to sodium mass-based ratio of 0.25, sulfate to chloride mass-based ratio of 0.14 [Pilson, 1998]). Given the large extension of sea ice at that site (up to 1600 km offshore the site), these values can be used as rough estimates for sea-salt aerosol purely produced by sea ice processes without contribution from the open ocean. Examining the degree of sulfate depletion relative to sodium (or chloride) in sea-salt particles collected at DDU on the impactor in the supermicron modes over the course of 2 years, Jourdain and Legrand [2002] calculated a mean winter sulfate to sodium mass-based ratio of 0.13 in 2000 and sulfate to chloride mass-based ratio of 0.06. Referring to the sulfate to sodium mass-based ratio of seawater (0.25) and assuming that the value of 0.07 derived at Neumayer reflects pure emissions from sea ice, we can estimate that on average 33% of sea salt comes from the open ocean at DDU in winter. The same calculation done with chloride (0.14 for open ocean against of 0.04 for sea ice) leads to a similar contribution of the open ocean (20%), both being consistent with model simulations. Finally, it is interesting to note that year-round impactor data gained at DDU suggest that greater presence of submicron sea-salt particles in winter than in summer (Figure 9). This feature is also broadly captured by model simulations, suggesting that the mechanism of sea-salt aerosol formation via sublimation of blowing salty snow particles, as formulated in Yang *et al.* [2008], is rational.

3.1.2. The Case of Concordia

As seen in Figures 5c and 5d, the concentrations of sodium are on average almost 50 times smaller at Concordia than at DDU. Though simulated concentrations exceed observations by a factor of 2 at DDU, the observed large gradient of sea-salt concentrations between DDU and Concordia is well simulated by the model. In summer, low values close to 5 ng m^{-3} or less are simulated, consistently with observations. In winter, although both observations and simulations indicate a large interannual variability, they show higher concentrations (up to 15 ng m^{-3} or more during the second half of winter) than over the rest of the year. As seen in Figure 5f, the model suggests that a similar fraction of winter sea-salt aerosol at Concordia comes from open ocean and sea ice. Though based on a limited impactor data set gained in 2006, Jourdain *et al.* [2008] confirmed the significant contribution (often dominant) of the sea-ice-sourced sea salt at Concordia in winter. We here report (Figure 10) the size-segregated composition of aerosol collected during 2 weeks in July 2011 during a strong marine advection event, as suggested by the high concentration of sodium (13 ng m^{-3}). The mean

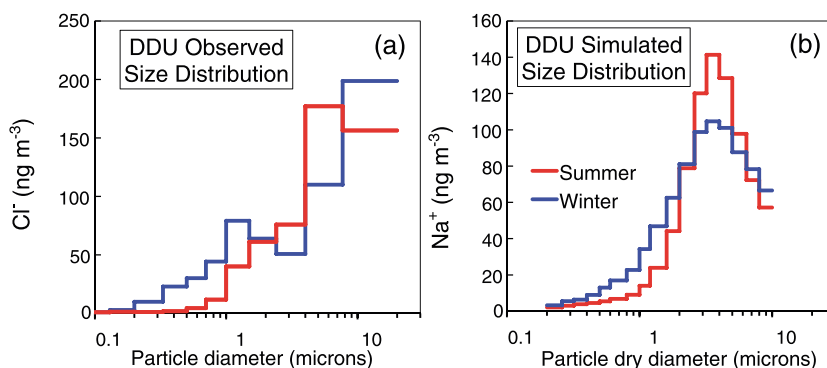


Figure 9. (a) Observed mean size-segregated content of chloride in aerosols collected at DDU in winter (blue) and summer (red) between January 1999 and August 2001. Winter concentrations (blue line) were multiplied by a factor of 2 to highlight the shift toward smaller particles. (b) Simulated mean size-segregated sea-salt particles (expressed as sodium concentrations) in winter and summer at DDU.

sulfate to sodium mass-based ratio observed on impactor stages having collected only sea salt and no aerosol of biogenic origin (i.e., particles having diameter ranging between 0.46 and 2.3 μm that contain no methanesulfonate, Figure 10d) is close to 0.13. This value indicates that on average during this period around 65% of sea salt was related to sea ice processes in rather good agreement with model simulations. Figures 5d and 5f indicates that whereas yearly mean model simulations ($9.6 \pm 4.2 \text{ ng m}^{-3}$) and observations ($6.7 \pm 5.1 \text{ ng m}^{-3}$) are quite consistent, the model overestimates concentrations during the first part of winter. In both observations and simulations, high variability from one winter to another winter can be seen, suggesting, as already discussed by *Levine et al.* [2014], that meteorological conditions play a key role on the low sea-salt concentration present over the Antarctic Plateau.

3.2. Observed Bromide Content of Aerosol

Ten day averaged concentrations of bromide in DDU bulk aerosol range from 0.05 to 11.8 ng m^{-3} ($2.4 \pm 1.9 \text{ ng m}^{-3}$, Figure 2a) with a well-marked maximum in January (Figure 11a). Given the corresponding sodium concentrations

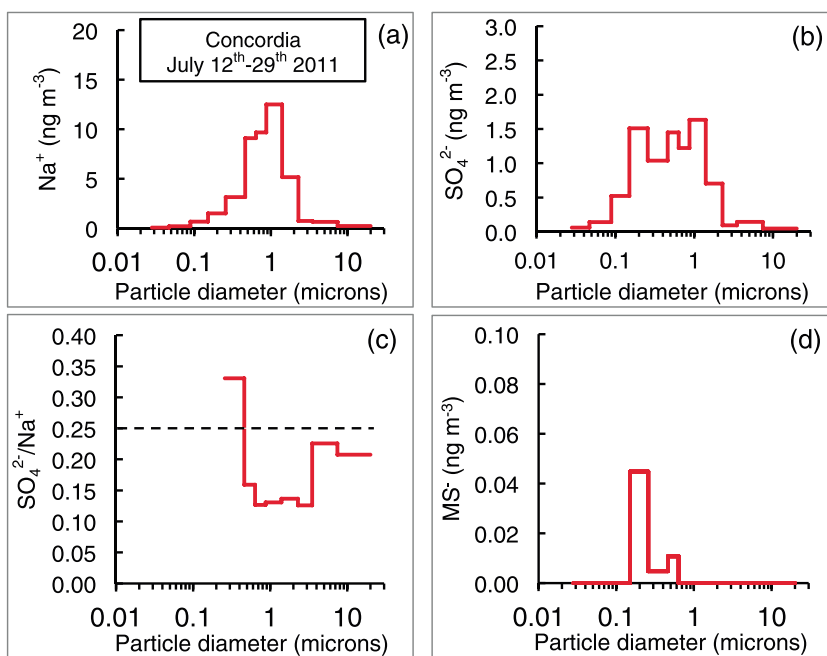


Figure 10. Observed size-segregated composition of aerosol collected at Concordia in July 2011: (a) sodium concentrations, (b) sulfate concentrations, (c) mass-based sulfate to sodium ratio, and (d) methanesulfonate concentrations. The dashed line in Figure 10c refers to the seawater ratio.

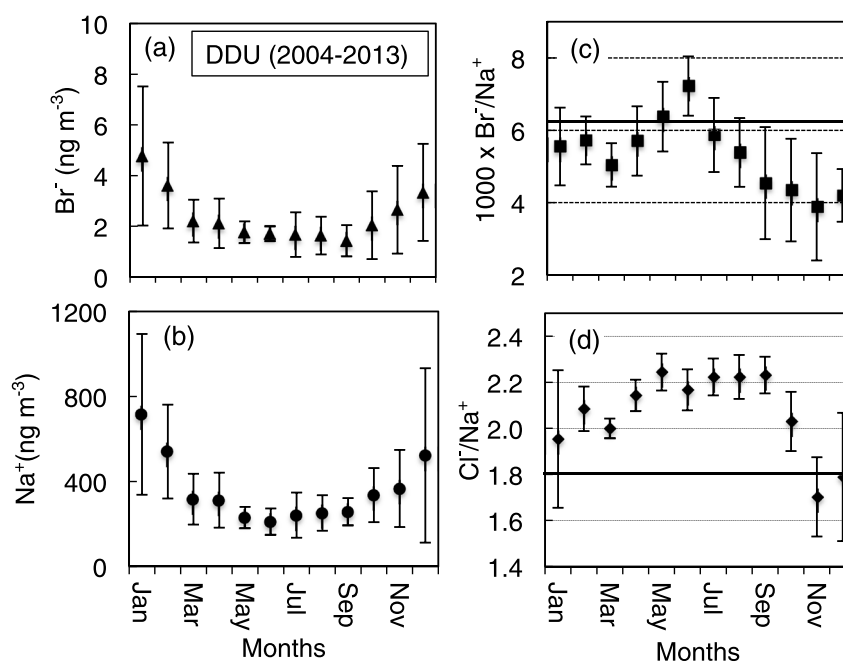


Figure 11. Monthly mean values of (a) bromide, (b) sodium, (c) bromide to sodium, and (d) chloride to sodium mass-based ratios in bulk aerosol, collected at DDU from January 2004 to December 2013.

($420 \pm 305 \text{ ng m}^{-3}$, Figure 2b) and the mass-based bromide to sodium ratio in seawater (6.25×10^{-3} , Pilsen [1998]), the range of bromide concentrations suggests sea salt as the main source of bromide in aerosol at DDU.

Whereas the overall relationship between bromide and sodium indicates a mean slope of 0.0061 in aerosol at DDU ($[\text{Br}^-] = 0.0061 [\text{Na}^+] + 0.14$, with $R^2 = 0.890$), Figures 2c and 11c show that the bromide to sodium mass-based ratio in aerosol at DDU is lower (4×10^{-3}) in summer and higher (7×10^{-3}) in winter than the seawater value. Such a depletion of bromide relative to sodium in summer is commonly observed at remote marine sites of the Southern Hemisphere [Sander *et al.*, 2003, and references therein]. Comparison of the bromide to sodium and chloride to sodium mass-based ratios over the course of the year (Figures 2 and 11) indicates that whereas the chlorine release only occurs in summer conditions, the bromine escape takes place most of time, except in midwinter. Considering the non-sea-salt sulfate and methanesulfonate concentrations that represent the two major acidic components of aerosol in these remote marine regions (equation (1) being not useful here due to local ammonia emissions from the large penguin colonies staying at the site), we found that whereas $[\text{nssSO}_4^{2-}] + [\text{MS}^-]$ remains close to $0.5 \mu\text{Eq L}^{-1}$ from mid-May to mid-September, values reach 6 to $8 \mu\text{Eq L}^{-1}$ in January (Figure 2e). Thus, the release of chlorine seems to require a more acidic character of aerosol than is the case for bromide that already escapes in September/October in spite of a far smaller acidity at that time compared to later in January (Figure 2e). In winter, the bromide to sodium mass-based ratio reaches a maximum value that slightly exceeds the seawater value of 6.25×10^{-3} (Figure 11c). As discussed in section 3.1, the observed strong depletion of sulfate relative to sodium implies a precipitation of mirabilite ($\text{Na}_2\text{SO}_4 \cdot 10\text{H}_2\text{O}$) on the sea ice surface at that season. Since halites precipitate well below -20°C (instead of -8°C for mirabilite) [Richardson, 1976], we may expect not only a lost of sulfate relative to sodium but also a lost a sodium relative to chloride and bromide. A mass balance calculation, done by assuming that the totality of sulfate (i.e., 0.25 Na) has been removed by mirabilite precipitation, permits to estimate an upper limit of the subsequent enrichment of halides relative to sodium. During the process, the corresponding lost of sodium accounts for 0.117 Na, increasing the chloride to sodium mass-based ratio of seawater from 1.8 to 2.1 (i.e., almost 20%).

On the basis of the bromide to sodium mass-based ratio observed in aerosol at DDU, we calculate in Table 3 monthly mean bromine depletion factor (DF) which represents the fraction of bromine having been lost from aerosol to the gas phase, DF being equal to $1 - [\text{Br}^-/\text{Na}^+]_{\text{aerosol}}/[\text{Br}^-/\text{Na}^+]_{\text{reference}}$. As discussed above, following Jourdain and Legrand [2002], we have assumed in DF calculations that at DDU sea-salt aerosol comes from open

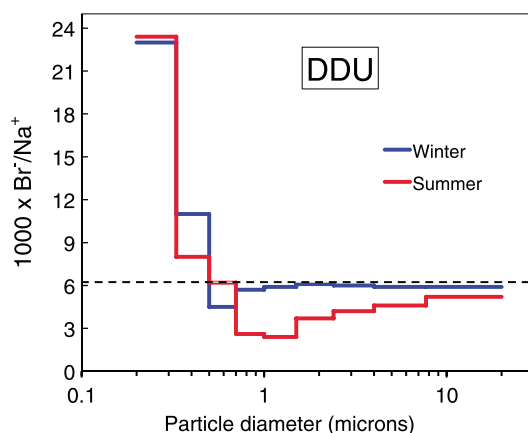


Figure 12. Size-segregated bromide to sodium mass-based ratio in aerosol collected at DDU in summer (red, 27–28 December 2000) and winter (blue, 19–24 June 2000). The dashed line refers to the bromide to sodium mass-based ratio in seawater.

clearly consistent with the one derived from the bulk aerosol continuous record. We can, however, notice a systematic tendency to have lower DF values on impactor than on bulk aerosol filters, especially in January and February. Two possibilities may explain such a difference. First, the presence of alkaline material trapped on bulk aerosol filters may have led to a positive artifact due to trapping of acidic gases like HBr, such a phenomenon being far less important on the impactor deposits. Detailed examination of the change of DF values and alkalinity of bulk aerosol filters does not support the significance of such a process. Also as previously discussed (see section 2.2), the good agreement found whatever the season for gaseous Br_y^* concentrations with mist chambers and denuders tubes suggests that the presence of alkaline material had not led to an underestimation of Br_y^* values from mist chambers for which a front filter was used. Since the mass of sodium or chloride in aerosol sampled by the impactor was found to be on average 50% smaller than the one sampled by the bulk filter, a second possibility to explain the lower DF values derived from impactors compared to bulk filters in January and February is that the open face filters used to collect bulk aerosol have sampled aerosols whose diameter exceeds $20\ \mu\text{m}$ (i.e., the cutoff size of the impactor). Given the expected lower DF values in very large particles compared to those in the medium size range of a few micron diameter [Sander *et al.*, 2003], the presence of very large particles in summer produced by open ocean near the DDU site may account for the difference in the DF values. Finally, as seen in Table 3, the DF values decreased in recent summers, during which (as previously discussed in section 3.1), smaller local emissions of large particles occurred due to the unusual presence of sea ice around the site.

At DDU, DF values reached a maximum from October to November (Table 3), consistent with previous studies conducted by Ayers *et al.* [1999] in the remote Southern Hemisphere site of Macquarie Island (55°S). The importance of the bromide depletion with respect to the size of aerosol was examined on the impactor samples. As seen in Figure 12, the depletion of bromide relative to sodium in summer aerosol at DDU with respect to the seawater composition is similar with what is observed at marine sites throughout the world. Indeed, the bromide to sodium mass-based ratio, which approaches the seawater value in large particles ($10\text{--}20\ \mu\text{m}$ diameter), decreases in particles of around $1\ \mu\text{m}$ diameter and always exceeds the seawater value in very small particles.

In contrast to what is observed at DDU, at Concordia the correlation between bromide and sodium is very poor and a relatively large y intercept is calculated by the linear regression ($[\text{Br}^-] = 0.0062 [\text{Na}^+] + 0.07$, with $R^2 = 0.2$). We failed to identify any significant correlation between bromide and other species (including tracers of dust like non-sea-salt calcium or potassium). Given uncertainty in measuring very low aerosol concentrations encountered over the Antarctic Plateau, more measurements are clearly needed to draw definite conclusions on the possible contribution of non-sea-salt sources (dust aerosol, contamination by station activities, and others) to the low background level of bromide at Concordia.

3.3. Near-Surface Gaseous Bromide

In contrast to bromine present in the aerosol phase whose concentrations decrease by more than one order of magnitude from the coast ($2.4 \pm 1.0\ \text{ng m}^{-3}$, Figure 11a) to inland ($0.11 \pm 0.13\ \text{ng m}^{-3}$, Figure 3b), the

ocean between November and March (i.e., a $[\text{Br}^-/\text{Na}^+]_{\text{reference}}$ value of 6.25×10^{-3}), whereas from May to October sea salt is mostly related to sea ice processes (i.e., $[\text{Br}^-/\text{Na}^+]_{\text{reference}}$ equal to 7.5×10^{-3}). For April we assumed an intermediate value of 6.9×10^{-3} . The DF values reported in Table 3 were derived from the mean seasonal cycle of bulk aerosol composition observed at DDU (Figure 11). Though based on limited impactor runs (by definition done under fine weather conditions to avoid problems with snow precipitation during sampling) the values DF values calculated from the impactor samplings indicate an overall seasonal change, which is

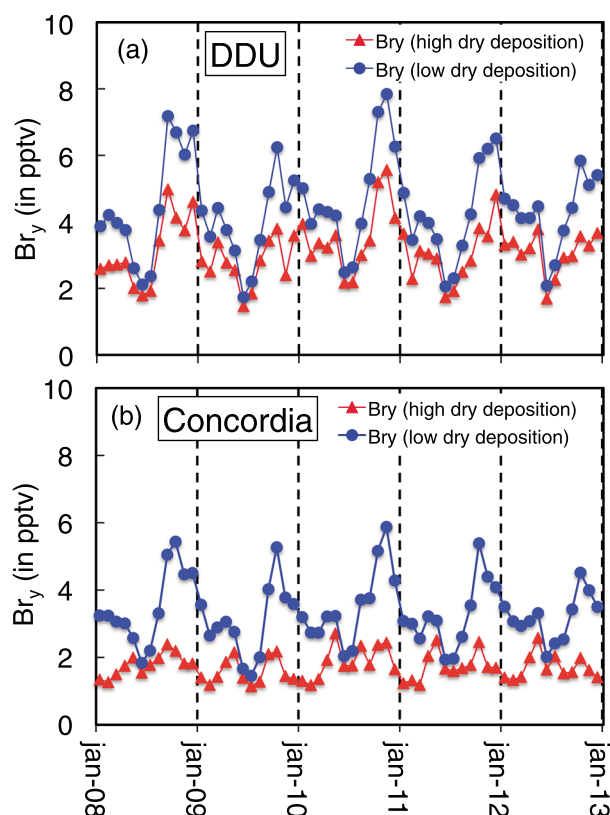


Figure 13. Simulated Br_y mixing ratios at (a) DDU and (b) Concordia when high and low dry deposition over snow and ice are assumed in the model (see section 3.3).

concentration of Br_y^* only decreases by a factor of 4 (from $9.7 \pm 3.8 \text{ ng m}^{-3}$ at DDU to $2.2 \pm 1.4 \text{ ng m}^{-3}$ at Concordia, Figure 4). In the original version of the model, only HBr and HOBr were dry deposited on snow and ice with velocities of 0.2 and 0.1 cm s^{-1} , respectively [Yang *et al.*, 2005]. With that, the model predicted a too small Br_y gradient between coastal ($4.3 \pm 1.4 \text{ pptv}$) and inland ($3.3 \pm 1.0 \text{ pptv}$) (Figure 13) suggesting a too weak deposition of Br_y over the Antarctic continent. Higher dry deposition velocities of Br_y were calculated by Parrella *et al.* [2012] who suggested mean global values close to 1 cm s^{-1} for HBr as well as for $BrONO_2$ and 0.4 cm s^{-1} for HOBr. As seen in Figure 13, simulations made using dry deposition rates for HBr, HOBr, and $BrONO_2$ on snow/ice of 1.0 , 0.5 , and 1.0 cm s^{-1} , respectively, indicate a decrease of simulated mixing ratios particularly at Concordia ($3.1 \pm 0.9 \text{ pptv}$ at DDU and $1.7 \pm 0.4 \text{ pptv}$ at Concordia) and an enhancement of the Br_y gradient between the coast and inland Antarctica. Note that the effect of increasing dry deposition in

the model mainly affects summer mixing ratios but not winter ones. As discussed below that is due to the fact that in winter the dominant Br_y species is Br_2 for which no dry deposition is assumed. In the following, simulations were made considering high dry deposition velocities over snow and ice for HBr, HOBr, and $BrONO_2$.

Figure 14 summarizes the simulated mixing ratios of Br_y and its partitioning at the two sites. In summer at DDU, the dominant species is HOBr, representing a third of Br_y , followed by BrO (29% of the total) and HBr (12%). At Concordia in summer HBr instead of HOBr is the dominant species (45% instead of 26% for HOBr), followed by BrO (24%). In winter, the absence of light makes Br_2 the dominant Br_y species at both sites (73% at DDU and more than 90% at Concordia). Such a dominance of HOBr, HBr, and BrO in summer and of Br_2 in winter is expected in typical polar environments (ozone above 1 ppbv and less than 5 pptv of NO_2) [Liao *et al.*, 2011, 2012a].

Observed Br_y^* concentrations are compared to simulations in Figure 15. As discussed in section 2.2, observed Br_y^* concentrations were compared to those of simulated Br_y and $Br_y - 0.4BrO - 1.1Br_2$. In summer at DDU, the observed Br_y^* concentrations (10.5 ng m^{-3}) are consistent with model simulations (11.4 ng m^{-3} for $[Br_y]$ and 8.6 ng m^{-3} for $[Br_y] - 0.6[BrO] - 1.1[Br_2]$). Note that concentrations simulated by applying the original low dry deposition velocities (16.7 ng m^{-3} for $[Br_y]$ and 12.8 ng m^{-3} for $[Br_y] - 0.6[BrO] - 1.1[Br_2]$) still remain in the range of observed Br_y^* concentrations. As seen in Figure 16, the effect of winds blowing from inland Antarctica in decreasing sea-salt concentrations at DDU (see section 3.1.1) is not observed for Br_y^* . This different feature between sea-salt aerosol and gaseous bromine is consistent with more homogeneous levels in marine and continental air masses for gaseous bromine than for sea-salt aerosol, partly linked to a relatively longer lifetime of Br_y of at least 5 days [Yang *et al.*, 2005; von Glasow *et al.*, 2004]. At Concordia, observed Br_y^* concentrations in summer (4 ng m^{-3}) are consistent with the model only when high deposition velocities of Br_y on ice are applied (4.9 ng m^{-3} for $[Br_y]$ and 4.2 ng m^{-3} for $[Br_y] - 0.6[BrO] - 1.1[Br_2]$ with high velocities against 12.1 ng m^{-3} for $[Br_y]$ and 10.5 ng m^{-3} for $[Br_y] - 0.6[BrO] - 1.1[Br_2]$ with low velocities).

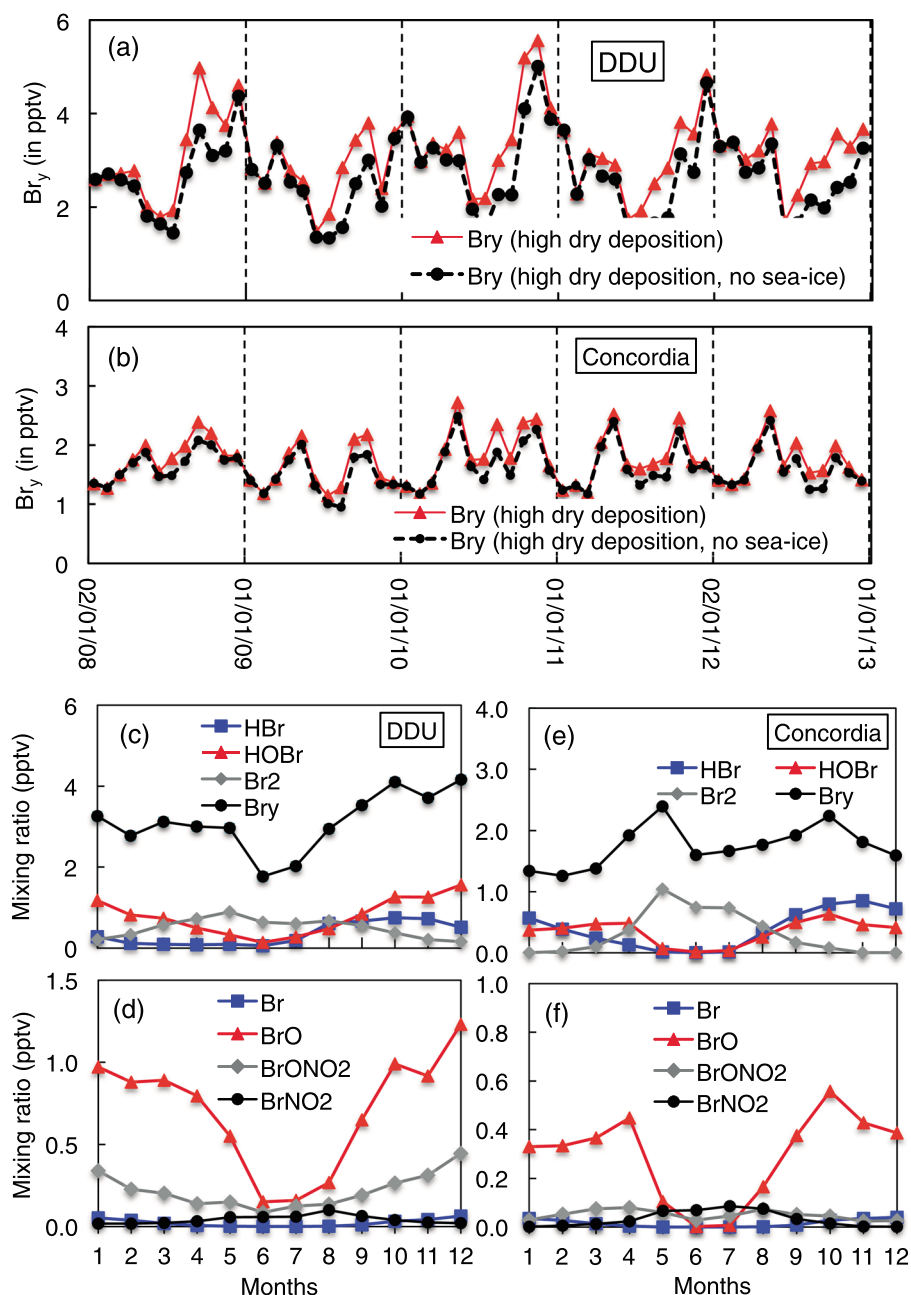


Figure 14. (a, b) Simulated mixing ratios of gaseous inorganic bromine and its partitioning at (c, d) DDU and (e, f) Concordia for 2008–2012.

In contrast, a winter minimum is clearly observed during the first part of the winter (May) at both sites, the annual minimum being simulated later (June–July) and being far less pronounced. The simulated gradient between the coast and the Antarctic Plateau (6.2 ng m^{-3} for $[\text{Br}_y]$ and 3.7 ng m^{-3} for $[\text{Br}_y] - 0.6[\text{BrO}] - 1.1[\text{Br}_2]$ at DDU against 5.3 ng m^{-3} for $[\text{Br}_y]$ and 2.7 ng m^{-3} for $[\text{Br}_y] - 0.6[\text{BrO}] - 1.1[\text{Br}_2]$ at Concordia) is weaker than observed (Br_y^* of 3.1 ng m^{-3} observed at DDU against 0.8 ng m^{-3} at Concordia). Among others, one possibility is that the model underestimates sinks of Br_2 , which dominates the Br_y family in winter Figures 14c and 14e. It has also to be emphasized that, as previously mentioned in section 3.1.2, the model largely overestimates the sea-salt concentrations during the first part of the winter at Concordia.

At both sites, observations show a minimum in May and a double maximum (Figure 15), a first one in late winter (August–September) and a second one in midsummer (January). In the case of DDU, this seasonal

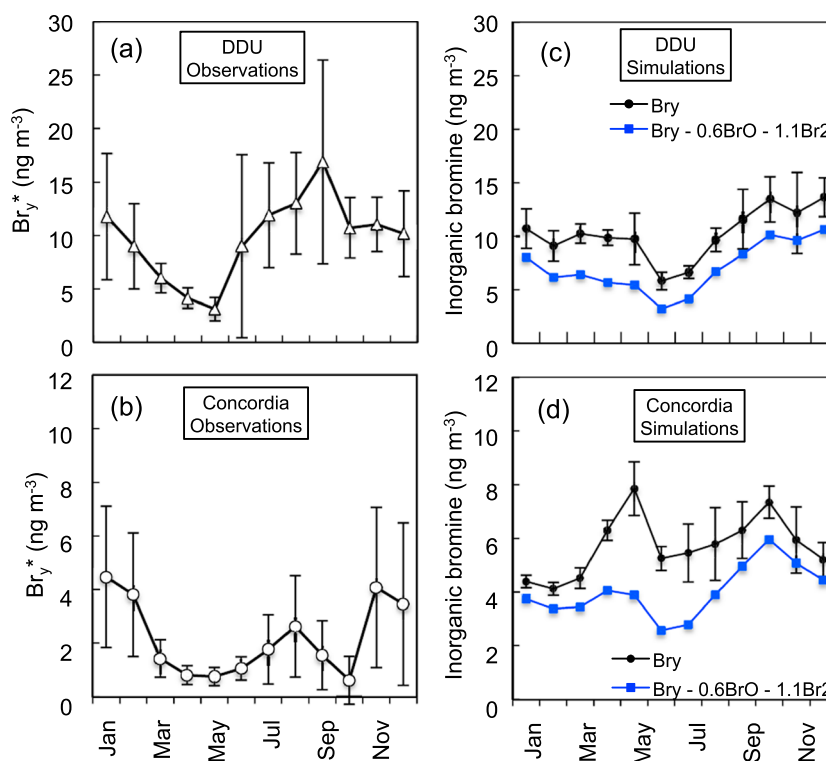


Figure 15. Monthly mean values of inorganic gaseous bromine (Br_y^*) observed (a) at DDU between 2006 and 2013 and (b) at Concordia between 2009 and 2014. Monthly mean concentrations of Br_y and $Br_y - 0.6BrO - 1.1Br_2$ (see equation (2)) simulated at (c) DDU and (d) Concordia. Vertical bars refer to day-to-day variability.

change is consistent with simulations and suggests a significant release of bromine related to both open ocean sea-salt emissions in summer and sea ice sea-salt emissions in late winter.

3.4. Other Processes That May Act as Bromine Sources

3.4.1. Mobile Coarse Sea-Salt Aerosol and Blowing Snow Particles

Whereas the release of bromide is expected to be weaker from the largest sea-salt particles than from smaller particles due to a shorter atmospheric lifetime and smaller surface/volume ratio limiting gas diffusion, coarse sea-salt aerosols still exhibit DF values slightly different from zero (DF close to 0.1 for particles of 20–40 μm ambient air diameter [Sander *et al.*, 2003]). Lieb-Lappen and Obbard [2015] recently investigated blowing snow samples collected on the coast of the Ross Sea and found that salty snow particles aloft at higher height (5.5 m) tend to lose more bromine than those at near-surface level. Thus, even with small bromide depletion, large salty particles such as blown snow and coarse sea-salt aerosol may still represent a significant source of Br_y . In another model run, in which coarse sea-salt aerosol (dry diameter ranging from 10 μm to 20 μm) and a DF value of 0.1 were considered, simulated Br_y concentrations at both DDU and Concordia were almost doubled (not shown), indicating large sea-salt particles could potentially play a role as a bromine source. Further field measurements are here needed to more precisely evaluate the contribution of these coarse salty particles as a source of bromine.

3.4.2. Snow Emissions

Model simulations have suggested that the photochemistry of bromide present in snow may make the snow pack of polar ice sheets a significant source of reactive Br_y . As seen in Table 2, both nitrate and bromide concentrations are strongly enhanced in the upper snow layers at Concordia. Such a strong increase of nitrate in surface snow layers was already reported by Röhrlsberger *et al.* [2000]. Based on nitrogen (¹⁵N) and (¹⁷O) isotopic composition of nitrate measured in the atmosphere and snow pits at Concordia, Frey *et al.* [2009] concluded that UV photolysis is an important process responsible for nitrate loss from snow as suggested by snow pit nitrate profiles. The similar increase of bromide concentrations seen near the snow surface (Table 2) also suggests a remobilization of bromide from the snow. Although the physical and chemical

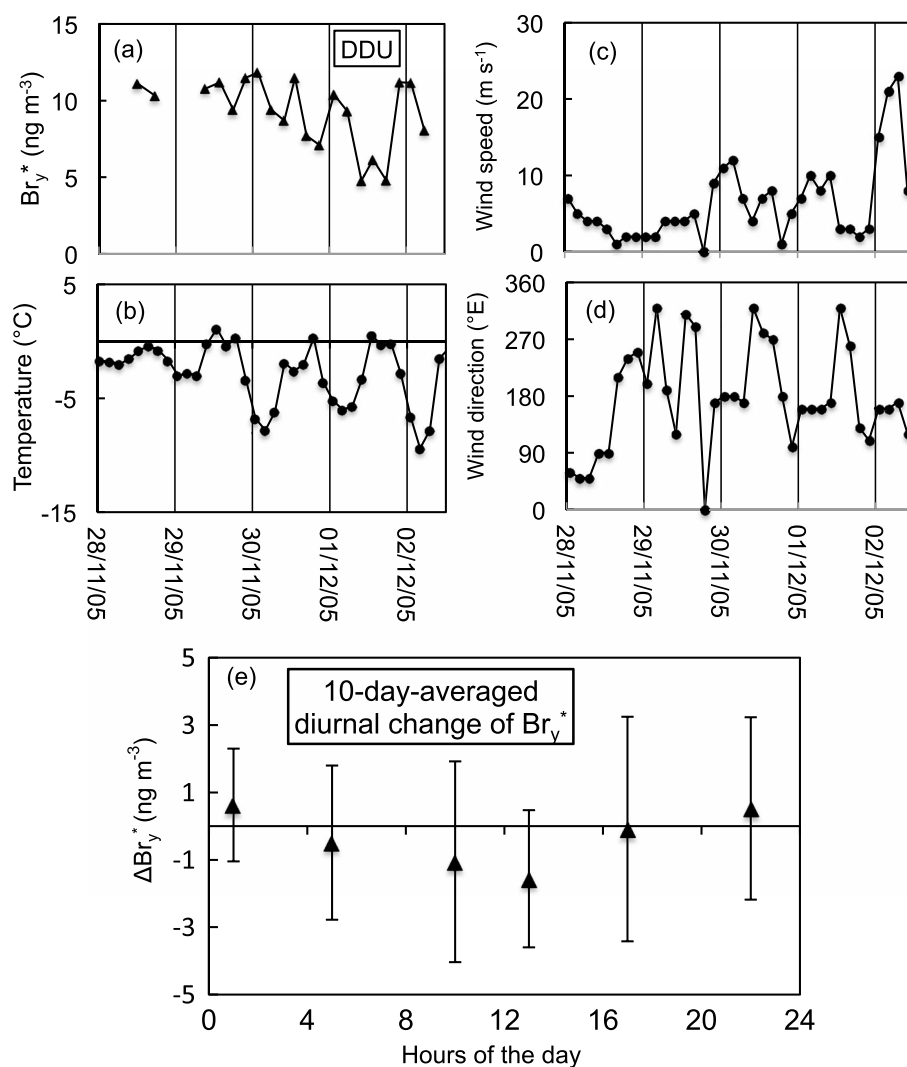


Figure 16. (a) Subdaily Br_y^* concentrations observed at DDU by using mist chamber sampling from 28 November to 2 December 2005 along with (b–e) weather conditions. (e) Mean residual change of Br_y^* with respect to the midnight values observed over 10 days (November–December 2005) characterized by changing wind conditions from continental at night to marine in the afternoon (so called sea breeze, see section 3.1).

properties of the liquid-like layer used in snow model simulations are not well known, *Thomas et al.* [2011] suggested that a few parts per trillion by volume of BrO as observed at Summit in central Greenland may be explained by emissions from the snow pack containing 10 nM (0.8 ppbw) as reported by *Dibb et al.* [2010].

In order to evaluate the possible role of a photochemical snowpack source at Concordia we ran an atmospheric 1-D transport model in which a Br_y emission from the snowpack (ϕ in molecules $m^{-2} s^{-1}$) is considered. The photochemical character of the Br_y snow source was considered by applying a diurnal variation to ϕ values. This was observed for photochemical emissions of NO_x from the snowpack at Concordia that ranged from 0.5×10^{13} molecules $m^{-2} s^{-1}$ at night to 3×10^{13} molecules $m^{-2} s^{-1}$ at noon [*Frey et al.*, 2015]. The model calculates the steady state Br_y mixing ratio by considering a dry deposition and a horizontal outflow from the system. For dry deposition on the snowpack, a deposition velocity of Br_y ranging from 0.2 to 1 $cm s^{-1}$ was applied (see discussions in section 3.3). In addition, to account for Br_y exchange within the atmosphere between gas and condensed (aerosols and hydrometeors) phases, we have assumed a Br_y lifetime of 5 days as typically reported for the free troposphere (5 days by *Yang et al.* [2005] and 10 days by *von Glasow et al.* [2004]). The Br_y lifetime related to horizontal export is calculated following *Jacob* [1999] by considering a grid length of 2000 km (similar to the size of East Antarctica) and a typical horizontal wind speed of 5 $m s^{-1}$ and

2 m s^{-1} at noon and midnight, respectively. A resulting Br_y lifetime relative to horizontal export of 2.5 days at noon and 10 days at midnight is obtained.

When the low dry deposition is considered a snow flux of $13 \times 10^{10} \text{ molecules m}^{-2} \text{ s}^{-1}$ ($2.4 \times 10^{10} \text{ molecules m}^{-2} \text{ s}^{-1}$ at night to $24 \times 10^{10} \text{ molecules m}^{-2} \text{ s}^{-1}$ at noon) is needed to explain a mean Br_y atmospheric mixing ratio of 1.7 pptv. That corresponds to a net snow-air flux of $5.9 \times 10^{10} \text{ molecules m}^{-2} \text{ s}^{-1}$ due to a recycling in snowpack by dry deposition ($7.1 \times 10^{10} \text{ molecules m}^{-2} \text{ s}^{-1}$). The net snow-air flux is only slightly changed ($5.6 \times 10^{10} \text{ molecules m}^{-2} \text{ s}^{-1}$) when it is assumed that the heterogeneous uptake of Br_y by aerosol and hydrometeors is ultimately deposited onto the snowpack. When a dry deposition velocity of 1 cm s^{-1} is considered, simulations indicate that a net snow-air flux of $6.5 \times 10^{10} \text{ molecules m}^{-2} \text{ s}^{-1}$ is required to account for observed 1.7 pptv of Br_y in the atmosphere. To maintain the 1.7 pptv of Br_y in the atmosphere over the three summer months, the snow at Concordia needs to emit 4.3 to $5.1 \times 10^{17} \text{ molecules m}^{-2}$ depending on the assumption made on the dry deposition velocity of Br_y on the snowpack. These values are more than 35 times higher than the inventory of bromide of snow ($0.12 \times 10^{17} \text{ molecules}$ present in the snow column of 1 m^2) calculated from measured depth profile of bromide and snow density (Table 2). Conversely, assuming that the total bromide content of snow, which is mainly located in the upper 10 cm and is thus available to photochemistry, is consumed over the three summer months (i.e., a net snow flux of $0.15 \times 10^{10} \text{ molecules m}^{-2} \text{ s}^{-1}$), we calculate a Br_y atmospheric mixing ratio of 0.05 pptv when a dry deposition velocity of 0.2 cm s^{-1} is assumed.

4. On the Importance of the Bromine Chemistry in Antarctica

In this section, we discuss the abundance of BrO (its mixing ratio near the surface as well as its vertical tropospheric column), which represents the inorganic bromine species that can significantly contribute to the overall oxidative property of the polar atmosphere.

4.1. Near-Surface BrO Mixing Ratios

Though limited to four days in summer 2011/2012 (from 31 January to 3 February), *Grilli et al.* [2013] reported BrO mixing ratios close to the detection limit of 2 pptv (or less) of the near-UV-Visible laser spectrometer deployed at DDU, being at least less than half of those reported by *Saiz-Lopez et al.* [2007] at Halley in summer (3 pptv). These limited observations available at DDU are consistent with the value of 1 pptv simulated for that site in January (Figure 14d).

At Concordia no direct surface measurements of BrO are yet available. Based on MAX-DOAS measurements made during sunny days in summer 2011/2012 at Concordia, *Frey et al.* [2015] estimated a BrO vertical column of $0.8 \times 10^{13} \text{ molecule cm}^{-2}$. Using this value, *Frey et al.* [2015] provided as a first estimate a BrO mixing ratio of 2 to 3 pptv near the surface during sunlight hours. Though the corresponding 24 h average values would be smaller, this estimate is 6 times larger than the simulated BrO value for Concordia in December/January (around 0.4 pptv, Figure 14f). Model simulations predicting that at Concordia in summer BrO would represent a third of the sum of other Br_y species, a mixing ratio of BrO of 2 to 3 pptv would imply the presence of 4 to 9 pptv of Br_y^* which also largely exceeds the observed and simulated Br_y^* values (Figure 15). *Frey et al.* [2015] pointed out larger mixing ratios in the free troposphere than in the near-surface layer at Concordia. This observation is consistent with our conclusion that the snowpack does not represent a significant source of inorganic bromine for the atmospheric boundary layer of the East Antarctic Plateau. Note that such a feature of the vertical distribution of BrO was also seen at the coastal Antarctic site of Halley in spring [*Roscoe et al.*, 2014].

4.2. Tropospheric BrO Vertical Column

In this section, we compare vertically integrated BrO concentration profiles from p-TOMCAT simulations with those from GOME-2 satellite observations. Both data sets are not directly comparable and several steps/corrections have been applied. First, the model output has been extracted at the overpass time of the satellite. Second, the modeled BrO profiles have been convolved with the averaging kernels of the satellite data, using the approach described in *Parrella et al.* [2012]. This step allows the direct comparison between the vertical columns from the model and the satellite. The averaging kernel informs on the measurement sensitivity in the different atmospheric layers and essentially provides the weight of the true BrO

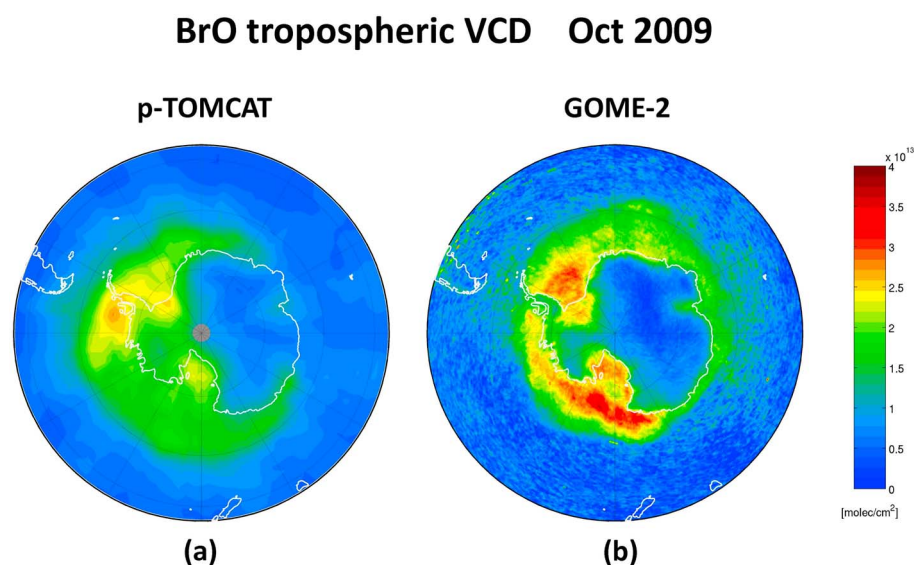


Figure 17. Comparison of (a) simulated and (b) observed BrO vertical tropospheric columns in October 2009.

concentration value at a given level to the retrieved vertical column. Third, a constant offset of 1.5×10^{13} molecules cm^{-2} has been subtracted from satellite BrO columns. There is increasing evidence for a probably ubiquitous free tropospheric BrO background [e.g., *Theys et al.*, 2011; *Parrella et al.*, 2012; *Wang et al.*, 2015, and references therein] with a typical vertical column of about this value. Although the uncertainty on the background BrO vertical column is significant, we have used a constant offset (1.5×10^{13} molecules cm^{-2}) as it also allows both satellite-based and modeled-based tropospheric BrO column having a similar open oceanic background (0.5 to 1×10^{13} molecules cm^{-2}) for a better comparison of the signals over the sea ice.

Figure 17 shows modeled and satellite-derived horizontal distributions of tropospheric BrO columns for October 2009. Both model and satellite columns are fairly consistent with low values (0.5 to 1×10^{13} molecules cm^{-2}) over inland East Antarctica, higher values (1.5 to 2×10^{13} molecules cm^{-2}) over inland West Antarctica, and highest values (1.5 to 2.5×10^{13} molecules cm^{-2}) on average over sea ice. There are however large differences over sea ice regions with satellite columns exceeding by 1 to 1.5×10^{13} molecules cm^{-2} the simulated BrO columns, in particular, over the Ross Sea and the Weddell Sea. Based on an extra simulation conducted without sea ice source (not shown), we found that the sea ice contribution to the total tropospheric BrO in October is relatively small, only 0.5 – 1.5×10^{13} molecules cm^{-2} , and mainly limited to the sea ice zone. This result is consistent with the surface Br_y simulation reported in Figure 11 showing that only 24% of Br_y originates in sea-ice-related processes. It can therefore be concluded that the model tends to underestimate tropospheric BrO column over sea ice. As discussed in section 3.4.1, mobile blowing snow particles as well as coarse sea-salt aerosol produced through the sublimation process can serve as potential bromine sources, neither of which was included in this simulation. Also, the bulk values of DF used to describe the bromine release south of 30°S were based on limited observations made at three sites (including DDU in this study). That represents another large source of uncertainty in formulating bromine emissions in this region where strong winds make the sea-salt production very large (nearly 40% of the global sea-salt production is calculated for regions located south from 30°S [*Yang et al.*, 2005]). In addition to these uncertainties on the bromine source, a better knowledge of the heterogeneous chemistry that takes place on sea-salt aerosol is certainly needed since it may affect (likely increase) the BrO partitioning in the Br_y family.

Figure 18 shows the monthly mean BrO tropospheric columns at DDU and Halley (averages for years 2008 and 2009) derived from p-TOMCAT model simulations and GOME-2 satellite observations. Both simulated and observed tropospheric BrO columns show a spring maximum around September–October, which is believed to be due to the polar “bromine explosion” effect. It is also seen that both simulations and satellite data are quantitatively consistent and suggest larger amounts of BrO at Halley compared to DDU.

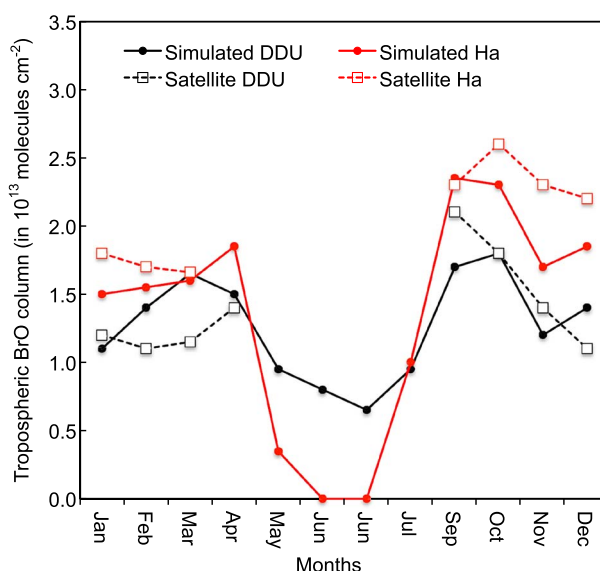


Figure 18. Simulated tropospheric BrO columns in the Antarctic sector of DDU ($66^{\circ}40'S$, $140^{\circ}01'E$) and Halley (Ha, $75^{\circ}35'S$, $26^{\circ}19'W$) and, when available, comparison with values derived from GOME-2 satellite observations. Each monthly value is the average for 2008 and 2009. All values are in 10^{13} molecules cm^{-2} .

efficient transport of inland air masses toward the coast there. These differences may impact the oxidizing properties of the atmosphere at these two coastal regions. In the following, we more precisely discuss this effect on the chemistry of dimethylsulfide (DMS) whose the oxidation represents one of the most abundant source of submicron aerosol in these regions.

The most efficient atmospheric oxidants of DMS are OH, BrO, and NO_3 , whereas others like Cl, IO, and O_3 are less efficient (see Barnes *et al.* [2006] for a review). In summer only OH and BrO may efficiently compete in oxidizing the DMS. Measurements of BrO made over one year at Halley by Saiz-Lopez *et al.* [2007] indicate a mean mixing ratio of 3 pptv during January–March. Such high BrO mixing ratios in summer make the BrO reaction on DMS producing DMSO 4 times faster than the one with OH (addition pathway) [Read *et al.*, 2008] whose concentrations reach 4×10^5 radicals cm^{-3} (24 h average) at that site [Bloss *et al.*, 2007]. At DDU, the importance of the HO_x chemistry was recently demonstrated by measurements of OH whose 24 h average concentrations reach 2.1×10^6 radicals cm^{-3} in summer [Kukui *et al.*, 2012]. Using these values and assuming the presence of 1.5 pptv of BrO in summer at DDU, we found that the OH addition production of DMSO is still 3 times faster than the one with BrO.

Concerning Concordia, with less than 1 pptv of BrO, it is clear that the bromine chemistry is far less efficient than the chemistry of OH for which Kukui *et al.* [2014] measured 24 h average concentrations of 3.1×10^6 radicals cm^{-3} in summer.

5. Conclusions

Several key aspects of the sea-salt aerosol (load, composition, and seasonality) at the coast and inland East Antarctica are established from multiyear observations derived from bulk and size-segregated samplings. At the coastal DDU site, the model predicts larger concentrations than observed but it is shown that a large part of the difference is related to local surface winds blowing often from the continent bringing sea-salt poor air to the site. At Concordia, observed annual mean concentrations close to 10 ng m^{-3} are well reproduced by the model. Whereas both observations and simulations show a sea-salt minimum in summer, the model simulates an enhancement of winter concentrations a few months earlier than generally observed. In spite of these discrepancies, at both sites in winter the simulated contribution of sea-ice-related process with respect to open ocean emissions (70% at DDU and 50% at Concordia) is consistent with conclusions drawn from the examination of the observed sulfate depletion relative to sodium with respect to seawater.

It should be noted that it is the first time (to our knowledge) that modeled and satellite BrO results are properly compared over the Antarctic regions and despite the differences discussed above, the results are encouraging and clearly illustrate the model skill in simulating the BrO explosion phenomenon.

4.3. Implications for the Oxidizing Property of the Antarctic Boundary Layer

Previous discussions have consistently shown that in summer, BrO is slightly more abundant at Halley compared to DDU, near the surface as well as within the entire troposphere. As already discussed by Legrand *et al.* [2009], the far larger surface ozone mixing ratios seen in summer at DDU compared to Halley suggest a more active HO_x chemistry due to a more

In summer, the estimated gaseous inorganic bromine mixing ratios derived from bromide measurements made in denuder tube extracts (10 and 4 ng m⁻³ at DDU and Concordia, respectively) are consistent with model simulations, suggesting sea salt as the main source of gaseous inorganic bromine species. In addition, it is shown that the observed bromide content of snow is not large enough to serve as a source able to maintain the observed gaseous inorganic bromine mixing ratios at Concordia in summer. In winter, simulations overestimate the gaseous inorganic bromine mixing ratios compared to observations, particularly at Concordia. In addition to an overestimation of sea-salt emissions by the model there, it is likely that a reason of the overestimate is related to the assumption of an absence of dry deposition for Br₂ (the dominant Br_y species in winter). More data are here needed in particular to better describe bromine source related to mobile particles (including blowing snow particles as well as sea-salt aerosol produced from both open ocean and sea ice). BrO simulations were also compared to data derived from GOME-2 satellite observations, both simulations and satellite data showing a larger tropospheric BrO abundance in spring as well as in summer over west coast compared to east coast of Antarctica. Finally, it is shown that whereas the bromine chemistry may largely compete with the OH chemistry at the West Antarctic coast, it is the case neither at the East coast nor over the Antarctic Plateau.

Acknowledgments

National financial support and field logistics supplies were provided by Institut Polaire Français-Paul Emile Victor (IPEV) within program 414 and 903 and the Agence Nationale de la Recherche through contract ANR-14-CE01-0001-01 (ASUMA). Aerosol data were obtained within the framework of the French environmental observation service CESOA (Etude du cycle atmosphérique du Soufre en relation avec le climat aux moyennes et hautes latitudes Sud, http://www-igge.ujf-grenoble.fr/CESOA/rubrique-que.php?id_rubrique=2) dedicated to the study of the sulfur cycle at middle and high southern latitudes and supported by the CNRS (INSU) and IPEV. We thank Météo France, who provided global irradiance and other basic meteorological parameters at DDU. Thanks to the Physical Sciences Division of the NOAA/OAR/ESRL PSD, Boulder, Colorado, USA, for NOAA_OI_SST_V2 sea ice data. We thank Bruno Jourdain from LGGE who assisted with preparations for the field campaigns. We thank Markus Frey from BAS who provide us typical values of salinity measured in blowing snow samples collected in the framework of the UK NERC-BLOWSEA project NE/J023051/1. We are also grateful to C. Legrand for good inspirations she gave us to finalize this rather long paper. Finally, we thank the three anonymous reviewers for their comments that improved data discussions. All surface data and corresponding model simulations presented in this paper are available at LGGE upon request (contact: legrand@lgge.obs.ujf-grenoble.fr or ps@lgge.obs.ujf-grenoble.fr). Other issues on model simulations are also available on request (contact: xinyang55@bas.ac.uk). The GOME-2 BrO data generated for this paper are available at BIRA-IASB (<http://uv-vis.aeronomie.be>) on request (contact: theys@aeronomie.be).

References

- Abbatt, J. P. D., et al. (2012), Halogen activation via interactions with environmental ice and snow, *Atmos. Chem. Phys.*, *12*, 6237–6271, doi:10.5194/acp-12-6237-2012.
- Abram, N. J., E. W. Wolff, and M. A. J. Curran (2013), A review of sea ice proxy information from polar ice cores, *Quat. Sci. Rev.*, *79*, 168–183, doi:10.1016/j.quascirev.2013.01.011.
- Adler, R. F., et al. (2003), The version-2 Global Precipitation Climatology Project (GPCP) monthly precipitation analysis (1979–present), *J. Hydrometeorol.*, *4*, 1147–1167.
- Ayers, G. P., R. W. Gillett, J. M. Cainey, and A. L. Dick (1999), Chloride and bromide loss from sea-salt particles in Southern Ocean air, *J. Atmos. Chem.*, *33*, 299–319.
- Barnes, I., J. Hjorth, and N. Mihalopoulos (2006), Dimethyl sulphide and dimethyl sulfoxide and their oxidation in the atmosphere, *Chem. Rev.*, *106*, 940–975.
- Bloss, W. J., J. D. Lee, D. E. Heard, R. A. Salmon, S.-J.-B. Bauguitte, H. K. Roscoe, and A. E. Jones (2007), Observations of OH and HO₂ radicals in coastal Antarctica, *Atmos. Chem. Phys.*, *7*, 4171–4185.
- Breider, T. J., M. P. Chipperfield, N. A. D. Richards, K. S. Carslaw, G. W. Mann, and D. V. Spracklen (2010), The impact of BrO on dimethylsulfoxide in the remote marine boundary layer, *Geophys. Res. Lett.*, *37*, L02807, doi:10.1029/2009GL040868.
- Caffrey, P. F., W. A. Hoppel, and J. J. Shi (2006), A one-dimensional sectional aerosol model integrated with mesoscale meteorological data to study marine boundary layer aerosol dynamics, *J. Geophys. Res.*, *111*, D24201, doi:10.1029/2006JD007237.
- Dibb, J. E., L. D. Ziemba, J. Luxford, and P. Beckman (2010), Bromide and other ions in the snow, firn air, and atmospheric boundary layer at Summit during GSHOX, *Atmos. Chem. Phys.*, *10*, 9931–9942, doi:10.5194/acp-10-9931-2010.
- Frey, M. M., J. Savarino, S. Morin, J. Erbland, and J. M. F. Martins (2009), Photolysis imprint in the nitrate stable isotope signal in snow and atmosphere of East Antarctica and implications for reactive nitrogen cycling, *Atmos. Chem. Phys.*, *9*, 8681–8696, doi:10.5194/acp-9-8681-2009.
- Frey, M. M., H. K. Roscoe, A. Kukui, J. Savarino, J. L. France, M. D. King, M. Legrand, and S. Preunkert (2015), Atmospheric nitrogen oxides (NO and NO₂) at Dome C, East Antarctica, during the OPALE campaign, *Atmos. Chem. Phys.*, *15*, 7859–7875, doi:10.5194/acp-15-7859-2015.
- Gallée, H., et al. (2015), Characterization of the boundary layer at Dome C (East Antarctica) during the OPALE summer campaign, *Atmos. Chem. Phys.*, *15*, 6225–6236, doi:10.5194/acp-15-6225-2015.
- Gallet, J.-C., F. Dominé, L. Arnaud, G. Picard, and J. Savarino (2011), Vertical profile of the specific surface area and density of the snow at Dome C and on a transect to Dumont d'Urville, Antarctica—Albedo calculations and comparison to remote sensing products, *Cryosphere*, *5*, 631–649, doi:10.5194/tc-5-631-2011.
- Gong, S. L. (2003), A parameterization of sea-salt aerosol source function for sub- and super-micron particles, *Global Biogeochem. Cycles*, *17*(4), 1097, doi:10.1029/2003GB002079.
- Grilli, R., M. Legrand, A. Kukui, G. Méjean, S. Preunkert, and D. Romanini (2013), First investigations of IO, BrO, and NO₂ summer atmospheric levels at a coastal East Antarctic site using mode-locked cavity enhanced absorption spectroscopy, *Geophys. Res. Lett.*, *40*, 791–796, doi:10.1002/grl.50154.
- Jacob, D. J. (1999), *Introduction to Atmospheric Chemistry*, 267 pp., Princeton Univ. Press, Princeton.
- Jones, A. E., P. Anderson, M. Begoin, N. Brough, M. Hutterli, G. Marshall, A. Richter, H. Roscoe, and E. Wolff (2009), BrO, blizzards, and drivers of polar tropospheric ozone depletion events, *Atmos. Chem. Phys.*, *9*, 4639–4652.
- Jourdain, B., and M. Legrand (2002), Year-round records of bulk and size-segregated aerosol composition and HCl and HNO₃ levels in the Dumont d'Urville (coastal Antarctica) atmosphere: Implications for sea-salt aerosol fractionation in the winter and summer, *J. Geophys. Res.*, *107*(D22), 4645, doi:10.1029/2002JD002471.
- Jourdain, B., S. Preunkert, O. Cerri, H. Castebrunet, R. Udisti, and M. Legrand (2008), Year-round record of size-segregated aerosol composition in central Antarctica (Concordia station): Implications for the degree of fractionation of sea-salt particles, *J. Geophys. Res.*, *113*, D14308, doi:10.1029/2007JD009584.
- König-Langlo, G., J. C. King, and P. Pettré (1998), Climatology of the three coastal Antarctic stations Dumont d'Urville, Neumayer, and Halley, *J. Geophys. Res.*, *103*, 10,935–10,946, doi:10.1029/97JD00527.
- Kukui, A., M. Legrand, G. Ancellet, V. Gros, S. Bekki, R. Sarda-Estève, R. Loisil, and S. Preunkert (2012), Measurements of OH and RO₂ radicals at the coastal Antarctic site of Dumont d'Urville (East Antarctica) in summer, *J. Geophys. Res.*, *117*, D12310, doi:10.1029/2012JD017614.
- Kukui, A., M. Legrand, S. Preunkert, M. Frey, R. Loisil, J. Gil Roca, B. Jourdain, M. King, J. France, and G. Ancellet (2014), OH and RO₂ measurements at Dome C, East Antarctica, *Atmos. Chem. Phys.*, *14*, 14,999–15,044.
- Legrand, M., F. Ducroz, D. Wagenbach, R. Mulvaney, and J. Hall (1998), Ammonium in coastal Antarctic aerosol and snow: Role of polar ocean and penguin emissions, *J. Geophys. Res.*, *103*, 11,043–11,056.

- Legrand, M., S. Preunkert, B. Jourdain, H. Gallée, F. Goutail, R. Weller, and J. Savarino (2009), Year round record of surface ozone at coastal (Dumont d'Urville) and inland (Concordia) sites in East Antarctica, *J. Geophys. Res.*, *114*, D20306, doi:10.1029/2008JD011667.
- Legrand, M., V. Gros, S. Preunkert, R. Sarda-Estève, A.-M. Thierry, G. Pépy, and B. Jourdain (2012), A reassessment of the budget of formic and acetic acids in the boundary layer at Dumont d'Urville (coastal Antarctica): The role of penguin emissions on the budget of several oxygenated volatile organic compounds, *J. Geophys. Res.*, *117*, D06308, doi:10.1029/2011JD017102.
- Legrand, M., S. Preunkert, M. Frey, T. Bartels-Rausch, A. Kukui, M. D. King, J. Savarino, M. Kerbrat, and B. Jourdain (2014), Large mixing ratios of atmospheric nitrous acid (HONO) at Concordia (East Antarctic Plateau) in summer: A strong source from surface snow?, *Atmos. Chem. Phys.*, *14*, 9963–9976, doi:10.5194/acp-14-9963-2014.
- Levine, J. G., X. Yang, A. E. Jones, and E. W. Wolff (2014), Sea salt as an ice core proxy for past sea ice extent: A process-based model study, *J. Geophys. Res. Atmos.*, *119*, 5737–5756, doi:10.1002/2013JD020925.
- Li, S.-M., Y. Yokouchi, L. A. Barrie, K. Muthuramu, P. B. Shepson, J. W. Bottenheim, W. T. Sturges, and S. Landsberger (1994), Organic and inorganic bromine compounds and their composition in the Arctic troposphere during polar sunrise, *J. Geophys. Res.*, *99*, 25,415–25,428.
- Liao, J., et al. (2011), A comparison of Arctic BrO measurements by chemical ionization mass spectrometry and long path-differential optical absorption spectroscopy, *J. Geophys. Res.*, *116*, D00R02, doi:10.1029/2010JD014788.
- Liao, J., et al. (2012a), Observations of inorganic bromine (HOBr, BrO, and Br₂) speciation at Barrow, AK in spring 2009, *J. Geophys. Res.*, *117*, D00R16, doi:10.1029/2011JD016641.
- Liao, J., et al. (2012b), Characterization of soluble bromide measurements and a case study of BrO observations during ARCTAS, *Atmos. Chem. Phys.*, *12*, 1327–1338, doi:10.5194/acp-12-1327-2012.
- Lieb-Lappen, R. M., and R. W. Obbard (2015), The role of blowing snow in the activation of bromine over first-year Antarctic sea ice, *Atmos. Chem. Phys.*, *15*, 7537–7545, doi:10.5194/acp-15-7537-2015.
- Long, M. S., W. C. Keene, R. C. Easter, R. Sander, X. Liu, A. Kerkweg, and D. Erickson (2014), Sensitivity of tropospheric chemical composition to halogen-radical chemistry using a fully coupled size-resolved multiphase chemistry–global climate system: Halogen distributions, aerosol composition, and sensitivity of climate-relevant gases, *Atmos. Chem. Phys.*, *14*, 3397–3425, doi:10.5194/acp-14-3397-2014.
- Maenhaut, W., R. Hillamo, T. Makela, J. L. Jaffrezou, M. H. Bergin, and C. I. Davidson (1996), A new cascade impactor for aerosol sampling with subsequent PIXE analysis, *Nucl. Instrum. Methods Phys. Res., Sect. B*, *109–110*, 482–487.
- Minikin, A., M. Legrand, J. Hall, D. Wagenbach, C. Kleefeld, E. Wolff, E. C. Pasteur, and F. Ducroz (1998), Sulfur-containing species (sulfate and methanesulfonate) in coastal Antarctic aerosol and precipitation, *J. Geophys. Res.*, *103*, 10,975–10,990.
- Munro, R., M. Eisinger, C. Anderson, J. Callies, E. Corpaccioli, R. Lang, A. Lefebvre, Y. Livschitz, and A. P. Albiñana (2006), GOME-2 on MetOp, paper presented at 2006 EUMETSAT Meteorological Satellite Conference, EUMETSAT, Helsinki, Finland.
- Parrella, J. P., et al. (2012), Tropospheric bromine chemistry: Implications for present and pre-industrial ozone and mercury, *Atmos. Chem. Phys.*, *12*, 6723–6740, doi:10.5194/acp-12-6723-2012.
- Pilson, M. E. Q. (1998), *An Introduction to the Chemistry of the Sea*, 2nd ed., 524 pp., Cambridge Univ. Press, New York.
- Rankin, A. M., V. Auld, and E. W. Wolff (2000), Frost flowers as a source of fractionated sea salt aerosol in the polar regions, *Geophys. Res. Lett.*, *27*, 3469–3472, doi:10.1029/2000GL011771.
- Rankin, A. M., E. W. Wolff, and S. Martin (2002), Frost flowers: Implications for tropospheric chemistry and ice core interpretation, *J. Geophys. Res.*, *107*(D23), 4683, doi:10.1029/2002JD002492.
- Rayner, N. A., D. E. Parker, E. B. Horton, C. K. Folland, L. V. Alexander, D. P. Rowell, E. C. Kent, and A. Kaplan (2003), Global analyses of sea surface temperature, sea ice, and night marine air temperature since the late nineteenth century, *J. Geophys. Res.*, *108*(D14), 4407, doi:10.1029/2002JD002670.
- Read, K. A., et al. (2008), DMS and MSA measurements in the Antarctic boundary layer: Impact of BrO on MSA production, *Atmos. Chem. Phys.*, *8*, 2657–2694.
- Reader, C., and N. McFarlane (2003), Sea-salt aerosol distribution during the Last Glacial Maximum and its implications for mineral dust, *J. Geophys. Res.*, *108*(D8), 4253, doi:10.1029/2002JD002063.
- Richardson, C. (1976), Phase relationship in sea ice as function of temperature, *J. Glaciol.*, *17*, 507–519.
- Ridley, B. A., et al. (2003), Ozone depletion events observed in the high latitude surface layer during the TOPSE aircraft program, *J. Geophys. Res.*, *108*(D4), 8356, doi:10.1029/2001JD001507.
- Roscoe, H. K., N. Brough, A. E. Jones, F. Wittrock, A. Richter, M. Van Roozendaal, and F. Hendrick (2014), Characterisation of vertical BrO distribution during events of enhanced tropospheric BrO in Antarctica, from combined remote and in-situ measurements, *J. Quant. Spectrosc. Radiat. Transfer*, *138*, 70–81.
- Röthlisberger, R., M. A. Hutterli, S. Sommer, E. W. Wolff, and R. Mulvaney (2000), Factors controlling nitrate in ice cores: Evidence from the Dome C deep ice core, *J. Geophys. Res.*, *105*, 20,565–20,572.
- Saiz-Lopez, A., A. S. Mahajan, R. A. Salmon, S. J.-B. Bauguitte, A. E. Jones, H. K. Roscoe, and J. M. C. Plane (2007), Boundary layer halogens in coastal Antarctica, *Science*, *317*, 348–351, doi:10.1126/science.1141408.
- Sander, R., et al. (2003), Inorganic bromine in the marine boundary layer: A critical review, *Atmos. Chem. Phys.*, *3*, 1301–1336, doi:10.5194/acp-3-1301-2003.
- Simpson, W. R., et al. (2007), Halogens and their role in polar boundary-layer ozone depletion, *Atmos. Chem. Phys.*, *7*, 4375–4418, doi:10.5194/acp-7-4375-2007.
- Smith, M. H., P. M. Park, and I. E. Consterdine (1993), Marine aerosol concentrations and estimated fluxes over the sea, *Q. J. R. Meteorol. Soc.*, *119*, 809–824, doi:10.1002/qj.49711951211.
- Sturges, W. T., R. C. Schnell, S. Landsberger, S. J. Oltmans, J. M. Harris, and S.-M. Li (1993), Chemical and meteorological influences on surface ozone destruction at Barrow, Alaska, during spring 1989, *Atmos. Environ.*, *27A*(17/18), 2851–2863.
- Theys, N., et al. (2011), Global observations of tropospheric BrO columns using GOME-2 satellite data, *Atmos. Chem. Phys.*, *11*, 1791–1811, doi:10.5194/acp-11-1791-2011.
- Thomas, J. L., J. Stutz, B. Lefer, L. G. Huey, K. Toyota, J. E. Dibb, and R. von Glasow (2011), Modeling chemistry in and above snow at Summit, Greenland—Part 1: Model description and results, *Atmos. Chem. Phys.*, *11*, 4899–4914, doi:10.5194/acp-11-4899-2011.
- von Glasow, R., R. Kuhlmann, M. G. Lawrence, U. Platt, and P. J. Crutzen (2004), Impact of reactive bromine chemistry in the troposphere, *Atmos. Chem. Phys.*, *4*, 2481–2497, doi:10.5194/acp-4-2481-2004.
- Wagenbach, D., F. Ducroz, R. Mulvaney, L. Keck, A. Minikin, M. Legrand, J. S. Hall, and E. W. Wolff (1998a), Sea-salt aerosol in coastal Antarctic regions, *J. Geophys. Res.*, *103*, 10,961–10,974, doi:10.1029/97JD01804.
- Wagenbach, D., M. Legrand, H. Fischer, P. Pichlmayer, and E. W. Wolff (1998b), Atmospheric near surface nitrate at coastal Antarctic sites, *J. Geophys. Res.*, *103*, 10,961–10,974.

- Wang, S., et al. (2015), Active and widespread halogen chemistry in the tropical and subtropical free troposphere, *Proc. Natl. Acad. Sci. U.S.A.*, doi:10.1073/pnas.1505142112.
- Warwick, N. J., J. A. Pyle, G. D. Carver, X. Yang, N. H. Savage, F. M. O'Connor, and R. A. Cox (2006), Global modeling of biogenic bromocarbons, *J. Geophys. Res.*, *111*, D24305, doi:10.1029/2006JD007264.
- Weller, R., D. Wagenbach, M. Legrand, C. Elsässer, X. Tian-Kunze, and G. König-Langlo (2011), Continuous 25-years aerosol records at coastal Antarctica: Part 1. Inter-annual variability of ionic compounds and links to climate indices, *Tellus, Ser. B*, *63*, 901–919, doi:10.1111/j.1600-0889.2011.00542.x.
- Yang, X., R. A. Cox, N. J. Warwick, J. A. Pyle, G. D. Carver, F. M. O'Connor, and N. H. Savage (2005), Tropospheric bromine chemistry and its impacts on ozone: A model study, *J. Geophys. Res.*, *110*, D23311, doi:10.1029/2005JD006244.
- Yang, X., J. A. Pyle, and R. A. Cox (2008), Sea salt aerosol production and bromine release: Role of snow on sea ice, *Geophys. Res. Lett.*, *35*, L16815, doi:10.1029/2008GL034536.
- Yang, X., J. A. Pyle, R. A. Cox, N. Theys, and M. Van Roozendael (2010), Snow-sourced bromine and its implications for polar tropospheric ozone, *Atmos. Chem. Phys.*, *10*, 7763–7773, doi:10.5194/acp-10-7763-2010.
- Yang, X., N. L. Abraham, A. T. Archibald, P. Braesicke, J. Keeble, P. J. Telford, N. J. Warwick, and J. A. Pyle (2014), How sensitive is the recovery of stratospheric ozone to changes in concentrations of very short lived bromocarbons?, *Atmos. Chem. Phys.*, *14*, 10,431–10,438, doi:10.5194/acp-14-10431-2014.